# ANALYTICAL STUDY ON ADHESIVELY BONDED JOINTS USING PEELING TEST AND SYMMETRIC COMPOSITE MODELS BASED ON BERNOULLI-EULER AND TIMOSHENKO BEAM THEORIES FOR ELASTIC AND VISCOELASTIC MATERIALS

A Thesis

by

YING-YU SU

Submitted to the Office of Graduate Studies of
Texas A&M University
in partial fulfillment of the requirements for the degree of

MASTER OF SCIENCE

December 2010

Major Subject: Mechanical Engineering

# ANALYTICAL STUDY ON ADHESIVELY BONDED JOINTS USING PEELING TEST AND SYMMETRIC COMPOSITE MODELS BASED ON BERNOULLI-EULER AND TIMOSHENKO BEAM THEORIES FOR ELASTIC AND VISCOELASTIC MATERIALS

A Thesis

by

YING-YU SU

Submitted to the Office of Graduate Studies of
Texas A&M University
in partial fulfillment of the requirements for the degree of

MASTER OF SCIENCE

Approved by:

| | |
|---|---|
| Chair of Committee, | Xin-Lin Gao |
| Committee Members, | Ibrahim Karaman |
| | Theofanis Strouboulis |
| Head of Department, | Dennis O'Neal |

December 2010

Major Subject: Mechanical Engineering

# ABSTRACT

Analytical Study on Adhesively Bonded Joints Using Peeling Test and Symmetric Composite Models Based on Bernoulli-Euler and Timoshenko Beam Theories for Elastic and Viscoelastic Materials. (December 2010)

Ying-Yu Su, B.S., National Chung Hsing University, Taichung, Taiwan

Chair of Advisory Committee: Dr. Xin-Lin Gao

Adhesively bonded joints have been investigated for several decades. In most analytical studies, the Bernoulli-Euler beam theory is employed to describe the behaviour of adherends. In the current work, three analytical models are developed for adhesively bonded joints using the Timoshenko beam theory for elastic material and a Bernoulli-Euler beam model for viscoelastic materials.

One model is for the peeling test of an adhesively bonded joint, which is described using a Timoshenko beam on an elastic foundation. The adherend is considered as a Timoshenko beam, while the adhesive is taken to be a linearly elastic foundation. Three cases are considered: (1) only the normal stress is acting (mode I); (2) only the transverse shear stress is present (mode II); and (3) the normal and shear stresses co-exist (mode III) in the adhesive. The governing equations are derived in terms of the displacement and rotational angle of the adherend in each case. Analytical solutions are obtained for the displacements, rotational angle, and stresses. Numerical

results are presented to show the trends of the displacements and rotational angle changing with geometrical and loading conditions.

In the second model, the peeling test of an adhesively bonded joint is represented using a viscoelastic Bernoulli-Euler beam on an elastic foundation. The adherend is considered as a viscoelastic Bernoulli-Euler beam, while the adhesive is taken to be a linearly elastic foundation. Two cases under different stress history are considered: (1) only the normal stress is acting (mode I); and (2) only the transverse shear stress is present (mode II). The governing equations are derived in terms of the displacements. Analytical solutions are obtained for the displacements. The numerical results show that the deflection increases as time and temperature increase.

The third model is developed using a symmetric composite adhesively bonded joint. The constitutive and kinematic relations of the adherends are derived based on the Timoshenko beam theory, and the governing equations are obtained for the normal and shear stresses in the adhesive layer. The numerical results are presented to reveal the normal and shear stresses in the adhesive.

# ACKNOWLEDGEMENTS

First and foremost, I would like to thank, gratefully and deeply, my advisor, Professor Xin-Lin Gao, whose patient, guidance, and encouragement enable me to pursue the research topic and complete this thesis.

I am also thankful to my committee members, Professor Ibrahim Karaman, Professor Theofanis Strouboulis, and Professor Amine Benzerga, for their time.

Finally, I would like to express my gratitude to my parents and friends, who always support me and give me unconditional love.

# TABLE OF CONTENTS

CHAPTER Page

## LIST OF FIGURES

FIGURE Page

# LIST OF TABLES

# CHAPTER I

# INTRODUCTION

## 1.1 Background

The use of adhesive joining in civil, aerospace and mechanical constructions has increased considerably in the last decade due to its advantages over traditional joining techniques such as mechanical fastening. The advantages include improved strength to weight ratios, increased overlap, increased service life, reduced cost and complexity, avoidance of additional stresses introduced by fastenings, higher efficiency, enhanced electrical insulation capabilities, and accommodation of thermal expansion mismatch.

The most common configuration of adhesively bonded joints is single-lap joints as shown in Fig. 1.1. It appears that the first single-lap adhesive joint design was proposed in Volkersen [1] by assuming that the adhesive deforms only in shear, while the adherend deforms only in tension. An improved design was later suggested in Goland and Reissner [2] by treating the adhesive layer as uniformly distributed tension and shear springs in the transverse direction. Since then, various types of adhesively bonded joints have been investigated. For instance, Hart-Smith [3] and Oplinger [4] developed a beam theory-based method to a single-lap joint.

---

This thesis follows the style of *International Journal of Adhesion & Adhesives*.

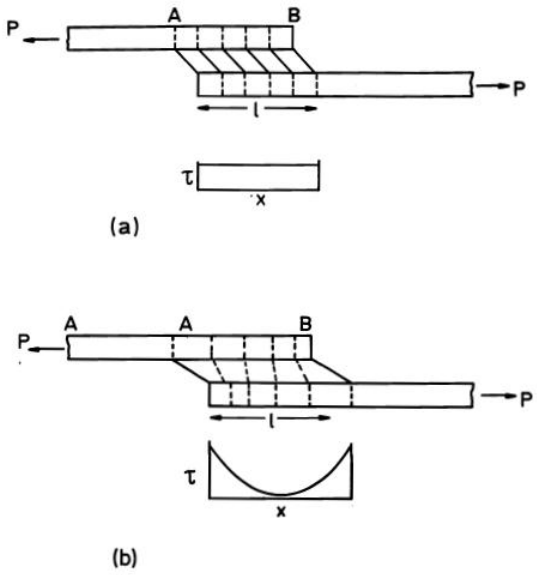


**Fig. 1.1** Schematic of a single-lap joint: (a) with rigid adherends; (b) with elastic adherends [5].

Two-dimensional 2-D elasticity was employed by Tsai and Morton [6] in their nonlinear finite element analysis of single-lap adhesive joints. Some studies of adhesive joint problems incorporate 2-D elasticity theories into variational methods. For example, the minimum strain energy method was applied by Adams and Peppiatt [7, 8], and the principle of complementary energy was employed in Allman [9] and Chen and Cheng [10]. The analysis of a single lap joint was further developed by accounting for the nonlinear [11] and elasto-plastic [12] responses of adherends. Recently, Mortensen and Thomsen [13] presented a unified approach for the analysis and design of adhesively bonded joints, Luo and Tong [14] proposed a higher-order displacement theory for stress analysis of a thick adhesive. Zou et al. [15] analyzed the adhesive stresses in adhesively

bonded symmetric composite and metallic joints based on the classical laminate theory and an adhesive interface constitutive model.

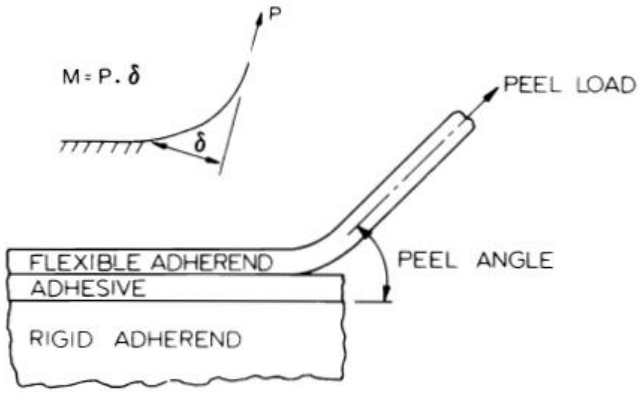


**Fig. 1.2** Schematic of a peeling test [16].

Various methods have been developed to determine the mechanical properties of adhesives. One method is the peeling test schematically shown in Fig.1.2, in which h a peeling is applied to separate the adherend from the substrate. Kaelble [17, 18] showed that bending moment is a crucial factor in determining fracture of an adhesive loaded in tension. Crocombe and Adams [19] used a large displacement finite element method to predict the peel strength. The trapezoidal cohesive zone model has been employed to examine normal and shear stresses in the fracture of adhesively bonded joints. Some analytical solutions for peeling based on the trapezoidal traction law were presented in Yamada [20], Williams and Hadavinia [21], Georgiou et al. [22] and Plaut and Ritchie [23].

In analyzing adhesively bonded joints, an adherends is usually modelled as a simple beam using various beam theories based on linear elasticity. However, viscoelastic beam models have hardly been employed to study adhesively bonded joints.

In deriving analytical solutions for adhesively bonded joint problems, the common approach is to construct a free body diagram at first. Constitutive relations depend on kinematic assumptions of a beam theory and material properties of adherends. Governing equations are reached by combing equilibrium equations and constitutive relations. Then, analytical solutions are derived for displacements, rotational angles and stresses in adhesively bonded joints.

## 1.2 Motivation

Adhesively bonded joints have been widely used because of their advantages over traditional joining methods. Despite significant advances in joining technology, the safety of joints in structures is still an issue, as about 70% of structure failures are initiated from joints [24]. Many studies on adhesively bonded joints have been performed using finite element methods or experimental approaches, each of which applies only to a given set of parameters and geometry. The cost in computing time and experiments can be significant. Therefore, analytical solutions that can be applied to adhesively bonded joints with various geometrical and loading conditions are desirable. This motivated the work presented here, which consists of two parts.

In most studies, an adherend is modeled as a Bernoulli-Euler beam based on classical elasticity. The Timoshenko beam theory takes into account shear deformation

and rotational inertia effects, making it suitable for describing the behavior of short beams. This has motivated the use of the Timoshenko beam theory in the first part of the current thesis work to derive analytical solutions for displacements and rotational angles in adhesively bonded joints under a peeling force and to obtain analytical solutions for adhesive stresses in symmetric composite adhesively bonded joints.

On the other hand, viscoelastic materials have been increasingly used in adhesive joints. However, no work has been reported using the Bernoulli-Euler beam theory or Timoshenko beam theory for viscoelastic materials to analytically study adhesively bonded joints. Therefore, in the second part of this thesis work, an adhesively bonded joint under peeling is analytically studied by treating the adherend as a viscoelastic Bernoulli-Euler beam.

### 1.3 Organization

The rest of this thesis is organized as follows:

The peeling test of an adhesively bonded joint is analytically studied in Chapter II by using the model of a Timoshenko beam on an elastic foundation. The adherend is considered as a Timoshenko beam, while the adhesive is taken to be a linearly elastic foundation. Three cases are considered: (1) only the normal stress is acting (mode I); (2) only the transverse shear stress is present (mode II); and (3) the normal and shear stresses co-exist (mode III) in the adhesive. The governing equations are derived in terms of the displacement and rotational angle of the adherend in each case. Analytical solutions are obtained for the displacements, rotational angle, and stresses. Numerical

results are presented to show the trends of the displacements and rotational angle changing with geometrical and loading conditions.

In Chapter III, the peeling test of an adhesively bonded joint is studied by using the model of a viscoelastic Bernoulli-Euler beam on an elastic foundation. The adherend is considered as a viscoelastic Bernoulli-Euler beam, while the adhesive is taken to be a linearly elastic foundation. Two cases under different stress history are considered: (1) only the normal stress is acting (mode I); and (2) only the transverse shear stress is present (mode II). The governing equations are derived in terms of the displacements. Analytical solutions are obtained for the displacements. The numerical results show that the deflection increases as time and temperature increase.

In Chapter IV, an analytical solution for a symmetric composite adhesively bonded joint is derived by considering the adherend as a Timoshenko beam. To extend the classical laminate theory, the constitutive and kinematic relations of the adherends are derived based on the Timoshenko beam theory and the governing equations are obtained for the normal and shear stresses in the adhesive layer. The analytically numerical results are presented to reveal the normal and shear stresses in the adhesive.

# CHAPTER II

# PEELING TEST OF AN ADHESIVELY BONDED JOINT BASED ON THE TIMOSHENKO BEAM THEORY

## 2.1 Introduction

The objective of this chapter is to develop a model for peeling of adhesively bonded joints using the Timoshenko beam theory. The adherend is considered as a Timoshenko beam, extending the work of Plaut and Ritchie [23] based on the Bernoulli-Euler beam theory. The Timoshenko beam theory takes into account shear deformation and rotational inertia, making it suitable for describing short beams, unlike the Bernoulli-Euler beam theory. The equilibrium equations are the same as those in Plaut and Ritchie [23] due to the same geometry and loading conditions, but the geometrical and constitutive equations are different.

A brief review of peeling tests on adhesively bonded joints is presented in Subsection 2.2. The basic formulation is described in Subsection 2.3, where the displacements are obtained by using the Timoshenko beam theory. In Subsection 2.4 and 2.5, the trapezoidal traction law used in Yang et al. [26-28], Thouless and Yang [29], and Wei and Hutchinson [30] is applied for the case with a negligible shear stress in the adhesive (mode I) and for the case with a negligible normal stress in the adhesive (mode II). In Subsection 2.6, the case with the same traction zone is applied to both a normal stress and a shear stress, in which the normal stress as a function of the vertical displacement has two linear distributions (with a positive slope and a negative slope,

respectively) and the shear stress as a function of the tangential displacement has two linear distributions (with a positive slope and a negative slope, respectively) as was done in Plaut and Ritchie [23]. The numerical results are quantitatively shown and discussed in Subsection 2.7.

**2.2 Peeling tests on adhesively bonded joints – a review**

The peeling test is a mechanical test, in which a thin flexible strip, called adherend, bonded to a substrate by an adhesive layer is pulled from the substrate by a peeling force. This test has been widely used for joint design purposes. The mechanics of the peeling test has been studied for decades. Chang [25] derived analytical solutions for the peeling force under different types of peeling of adhesive joints, with the peeling force applied perpendicularly. The adhesive stress distribution changing with the angle of peeling has been investigated by Kaelble [18]. Crocombe and Adams [19] used a large displacement finite-element technique to predict the peel strength.

Most studies on adhesive joints used fracture mechanics to predict failure [31-33]. Several analytical solutions for peeling with the trapezoidal traction law were presented in Yamada [20], Williams and Hadavinia [21], Georgiou [22] and Plaut and Ritchie [23]. The traction-separation relationship was assumed to be piecewise linear, with an initially positive slope (elastic behavior), followed by constant slope (perfectly plastic behavior), and finally a negative slope (damage behavior) (Williams and Hadavinia [21]).

**2.3 Formulation based on the Timoshenko beam theory**

Consider the peeling test model shown in Fig. 2.1, where a tape is peeled from a rigid substrate. This configuration was also used by Plaut and Ritchie [23] in their study based on the Bernoulli-Euler beam theory. The tape that is adhered to the substrate is considered as a fixed end-free end, linearly elastic and uniform Timoshenko beam. In Fig. 2.1, $L$ is the original length of the adhesive and adherend. In the shaded region ($-L < x < 0$), the adhesive is assumed to be linearly elastic, and in the dotted region (from $x = 0$ to the peel front) the adhesion is governed by constant or linearly decreasing traction laws. In Fig. 2.1, $M_o$ denotes the resultant bending moment, $F_x$ and $F_y$ represent, respectively, the horizontal component and vertical component of the resultant force, $F_x$, $F_y$ and $v(x)$ stands for the vertical displacement of the centreline of the tape and is positive if upward. The applied forces are such that $v > h_a$. The slope of the deformed centreline of the tape is assumed to be small.

The equilibrium of moments and forces shown in the free-body diagram in Fig. 2.2 leads to

$$\frac{dM}{dx} = P\frac{dv}{dx} - Q + \frac{1}{2}wh_b\tau, \tag{2.1}$$

$$\frac{dP}{dx} = w\tau, \tag{2.2}$$

$$\frac{dQ}{dx} = wS. \tag{2.3}$$

where $\tau = \tau(x)$ and $S = S(x)$ are, respectively, the shear stress and normal stress on the interface between the tape and the substrate, and $P, Q, M$ are, respectively, the normal force, shear force, and bending surface acting on the *x*- cross section of the tape.

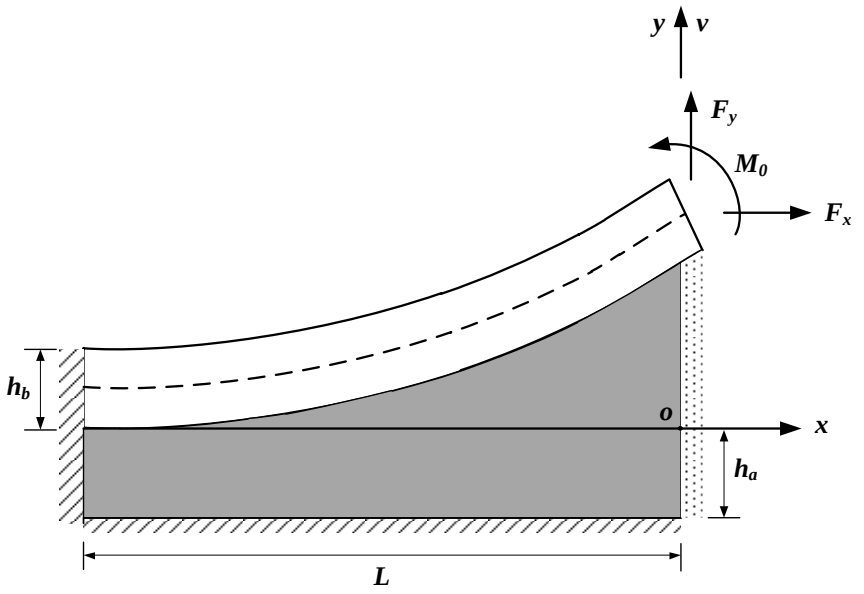


**Fig. 2.1** Schematic of a tape peeling test.

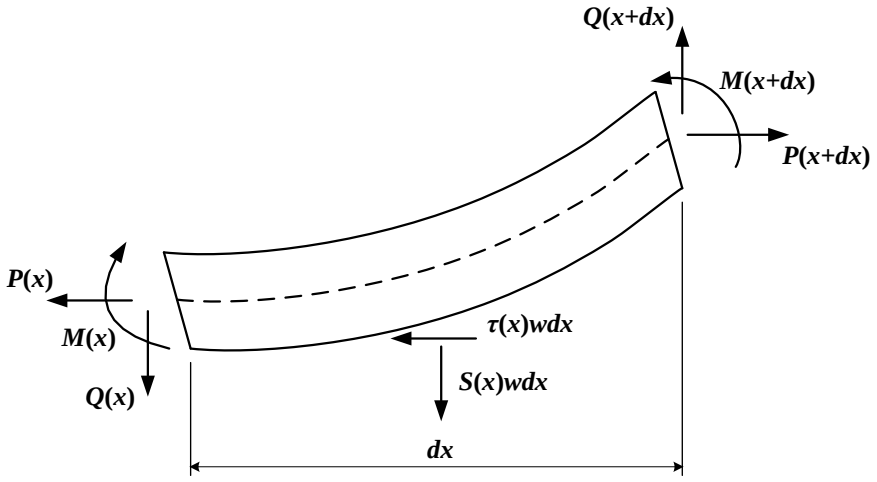


**Fig. 2.2** Free-body diagram of the tape differential element with length dx.

The constitutive equations based on the classical Timoshenko beam theory can be described by (Ma, Gao and Reddy [34])

$$P = E_b w h_b \frac{du}{dx}, \quad M_x = E_b I_b \frac{d\phi}{dx}, \quad Q = K_s \mu A \left(-\phi + \frac{dv}{dx}\right), \qquad (2.4a\text{-}c)$$

where $h_b, w, A_b, E_b, I_b$ are, respectively the tape thickness, backing width, cross-sectional area (with $A = h_b w$), Young's modulus and second moment of cross-sectional area (with $I_b \equiv I_z = \frac{1}{12} h_b^3 w$). Also, $h_a$ is the initial adhesive thickness, and $E_a, G_a$ are the Young's modulus and shear modulus of the adhesive.

**2.4 Loading Mode I**

In this subsection it is assumed that the horizontal forces are negligible so that $F_x = 0$, $P = 0$ and $\tau = 0$. From Eqs. (2.1) and (2.3), it then follows that

$$M' + Q = 0, \qquad (2.5)$$

$$Q' = wS. \qquad (2.6)$$

noting that Eq. (2.2) is identically satisfied.

Substituting Eqs. (2.4a-c) into Eqs. (2.5) and (2.6), gives

$$E_b I_b \phi''' + wS = 0, \qquad (2.7)$$

$$K_s \mu A(-\phi' + v'') - wS = 0. \qquad (2.8)$$

In this case, $v$ is denoted by $v_1$, $v_2$ and $v_3$, respectively, for $x < 0$ (linear elastic adhesive), $0 < x <$ r (perfectly plastic adhesive), and $r < x < q$ (damage region), as shown in Fig. 2.3(a). The values of the vertical displacement $v$ at $x = 0$, $r$ and $q$ are

denoted by $c$, $e$ and $d$, respectively. The normal stress $S$ as a function of $v$ is depicted in Fig. 2.3(b) and is given by

$$S(v) = \frac{k}{w} v_1, \quad x < 0; \tag{2.9a}$$

$$S(v) = \frac{k}{w} c, \quad 0 < x < r; \tag{2.9b}$$

$$S(v) = \frac{k}{w} c(d - v_3)/(d - e), \quad r < x < q, \tag{2.9c}$$

where the substrate stiffness is defined by $k = E_a w / h_a$ [23].

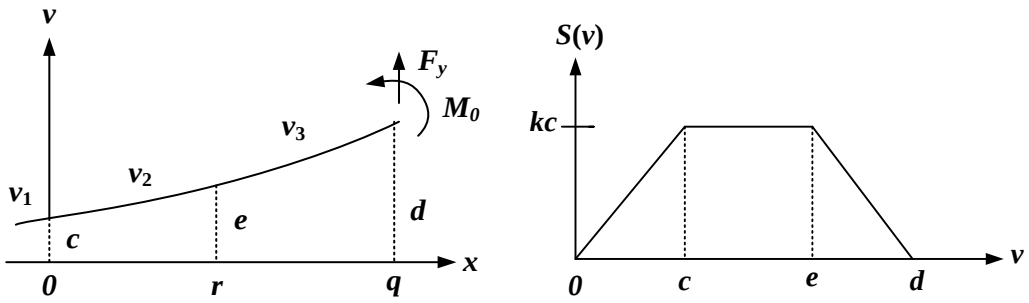


(a) (b)

**Fig. 2.3** Loading in Mode I: (a) vertical displacement of the tape; (b) normal stress as a function of the vertical displacement [23].

### *2.4.1 Solution in the first region: $x < 0$*

Using Eq. (2.9a) in Eqs. (2.7) and (2.8) yields

$$\phi''' = -\frac{k}{E_b I_b} v_1, \tag{2.10}$$

$$-k_s \mu A \phi' + k_s \mu A v_1'' - k v_1 = 0. \tag{2.11}$$

Differentiating Eq. (2.11) twice and substituting Eq. (2.10) into the resulting equation will lead to

$$A_1 v_1'''' - A_2 v_1'' + A_3 v_1 = 0, \tag{2.12a}$$

where

$$A_1 \equiv k_s \mu A,\ A_2 \equiv k,\ A_3 \equiv \frac{A_1 A_2}{E_b I_b}. \tag{2.12b}$$

The general solution of Eq. (2.12a) can be obtained as

$$v_1(x) = a_1 e^{\alpha_1 x} + a_2 e^{-\alpha_1 x} + a_3 e^{\beta_1 x} + a_4 e^{-\beta_1 x}, \tag{2.13a}$$

where $a_1 \sim a_4$ are four constants, and

$$\alpha_1 \equiv \sqrt{\frac{A_2 + \sqrt{{A_2}^2 - 4A_1A_3}}{2A_1}},\ \beta_1 \equiv \sqrt{\frac{A_2 - \sqrt{{A_2}^2 - 4A_1A_3}}{2A_1}}. \tag{2.13b}$$

If ${A_2}^2 - 4A_1A_3 \geq 0$ or $k \geq \frac{4{k_s}^2\mu^2A^2}{E_bI_b}$, then $\alpha_1$, $\beta_1$ are real, and $v_1(x)$ given in Eq. (2.13a) is an exponential function.

Substituting Eqs. (2.13a) into (2.10) gives the rotation angle as

$$\phi_1(x) = -\frac{A_3 a_1}{A_1 {\alpha_1}^3} e^{\alpha_1 x} + \frac{A_3 a_2}{A_1 {\alpha_1}^3} e^{-\alpha_1 x} - \frac{A_3 a_3}{A_1 {\beta_1}^3} e^{\beta_1 x} + \frac{A_3 a_4}{A_1 {\beta_1}^3} e^{-\beta_1 x} + \frac{1}{2} a_5 x^2 + a_6 x + a_7, \tag{2.14}$$

where $a_5 \sim a_7$ are three additional constants.

### *2.4.2 Solution in the second region:* $0 < x < r$

Inserting Eq. (2.9b) into Eqs. (2.7) and (2.8) gives

$${\phi_2}''' = -\frac{kc}{E_bI_b}, \tag{2.15}$$

$$-k_s\mu A{\phi_2}' + k_s\mu A v_2'' - kc = 0. \tag{2.16}$$

Differentiating Eq. (2.16) twice and then substituting Eq. (2.15) into the resulting equation yields

$$\frac{kc}{E_b I_b} + v_2'''' = 0. \tag{2.17}$$

The general solution of Eq.(2.17) is

$$v_2(x) = -\frac{kc}{24E_b I_b}x^4 + \frac{a_8}{6}x^3 + \frac{a_9}{2}x^2 + a_{10}x + a_{11}\,, \tag{2.18}$$

where $a_8$~$a_{11}$ are constants.

From Eq. (2.15), it follows that

$$\phi_2(x) = -\frac{kc}{6E_b I_b}x^3 + \frac{a_{12}}{2}x^2 + a_{13}x + a_{14}\,, \tag{2.19}$$

where $a_{12}$~$a_{14}$ are additional constants.

***2.4.3 Solution in the third region:*** r < x < q

Substituting Eq. (2.9c) into Eqs. (2.7) and (2.8) results in

$$\phi_3''' = -\frac{kc(d-v_3)}{E_b I_b(d-e)}, \tag{2.20}$$

$$-k_s\mu A\phi_3' + k_s\mu A v_3'' - \frac{kc(d-v_3)}{(d-e)} = 0. \tag{2.21}$$

Differentiating Eq. (2.21) twice and substituting Eq. (2.20) into the resulting equation gives

$$A_4 v_3'''' + A_5 v_3'' + A_6 v_3 = A_7, \tag{2.22a}$$

where

$$A_4 = k_s\mu A,\ A_5 = \frac{kc}{(d-e)},\ A_6 = -\frac{k_s\mu Akc}{E_b I_b(d-e)},\ A_7 = -\frac{k_s\mu Akcd}{E_b I_b(d-e)}. \tag{2.22b}$$

Then, the general solution is

$$v_3(x) = d + a_{15}\cos\gamma x + a_{16}\sin\gamma x + a_{17}\cos\xi x + a_{18}\sin\xi x, \tag{2.23a}$$

where $a_{15}$~$a_{18}$ are constants, and

$$\gamma \equiv \sqrt{\frac{A_5-\sqrt{{A_5}^2-4A_4A_6}}{2A_4}}, \qquad \xi \equiv \sqrt{\frac{A_5+\sqrt{{A_5}^2-4A_4A_6}}{2A_4}}. \tag{2.23b}$$

Substituting Eq. (2.23a) into Eq. (2.20) leads to

$$\phi_3(\mathrm{x}) = -\frac{kc}{E_b I_b(d-e)}\left(\frac{\mathrm{a}_{15}}{\gamma^3}\sin\gamma x - \frac{\mathrm{a}_{16}}{\gamma^3}\cos\gamma x + \frac{\mathrm{a}_{17}}{\xi^3}\sin\xi x - \frac{\mathrm{a}_{18}}{\xi^3}\cos\xi x\right). \tag{2.24}$$

**2.5 Loading Mode II**

In this loading mode, only the applied horizontal force $F_x$ and the associated shear stress $\tau$ are considered, and $F_y, M_o, Q, M$ and $S$ are all taken to be zero. The equilibrium equations given in Eqs. (2.1)-(2.3) then become

$$Pv' = -\frac{1}{2}wh_b\tau, \tag{2.25a}$$

$$P' = w\tau, \tag{2.25b}$$

and the constitutive equations listed in Eqs. (2.4a-c) now read

$$P = E_b w h_b \frac{du}{dx}, \tag{2.26a}$$

$$\frac{d\phi}{dx} = 0, \tag{2.26b}$$

$$\phi = \frac{dv}{dx}, \tag{2.26c}$$

where $u(x)$ denotes the horizontal displacement of a point on the centroidal axis and is positive in the *x* direction.

As shown in Fig. 2.4(a), the values of $u(x)$ at *x=0*, $r$ and $q$ are denoted by $\eta, \Delta$ and $\rho$ respectively, and the subscripts 1, 2, and 3 stands for quantities in the elastic, plastic, and damage regions, respectively. As shown in Fig. 2.4(b), the shear stress $\tau$ is a function of the horizontal displacement and is given by

$$\tau_1(u) = G_a \frac{u_1}{h_a}, \quad x < 0; \tag{2.27a}$$

$$\tau_2(u) = G_a \frac{\eta}{h_a}, \quad 0 < x < r; \tag{2.27b}$$

$$\tau_3(u) = \frac{G_a \eta(\rho - u_3)}{h_a(\rho - \Delta)}, \quad r < x < q. \tag{2.27c}$$

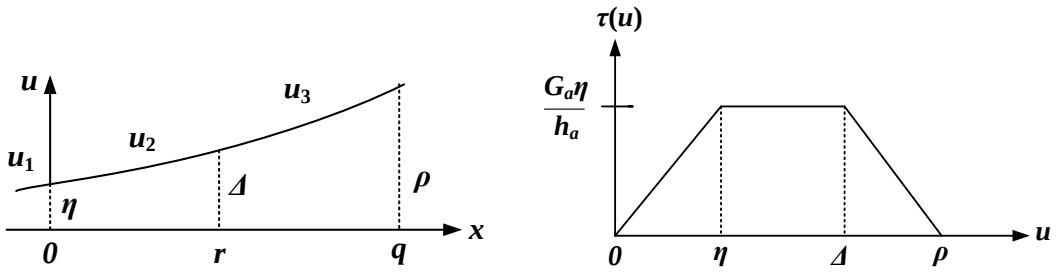


(a) (b)

**Fig. 2.4** Loading in Mode II: (a) horizontal displacement; (b) shear stress as a function of the horizontal displacement [23].

### *2.5.1 Solution in the first region: $x < 0$*

Substituting Eq. (2.27a) into Eq. (2.25b) gives

$$P_1' = wG_a \frac{u_1}{h_a}. \tag{2.28}$$

Note that Eq. (2.26a) can also be rewritten as

$$\frac{du}{dx} = \frac{P}{E_b w h_b}. \tag{2.29}$$

Differentiating Eq. (2.28) and substituting Eq. (2.29) into the resulting equation will yield

$$P_1'' - {\alpha_2}^2 P_1 = 0, \tag{2.30a}$$

where

$${\alpha_2}^2 \equiv \frac{G_a}{h_a h_b E_b}. \tag{2.30b}$$

The general solution of Eq. (2.30a) is

$$P_1(x) = a_{19} e^{\alpha_2 x} + a_{20} e^{-\alpha_2 x}, \tag{2.31a}$$

where $a_{19}$ and $a_{20}$ are two constants.

Using Eq. (2.31a) in Eq. (2.29) and integrating the resulting equation will give

$$u_1(x) = \frac{1}{E_b w h_b}\left(\frac{a_{19}}{\alpha_2} e^{\alpha_2 x} - \frac{a_{20}}{\alpha_2} e^{-\alpha_2 x}\right) + a_{21}, \tag{2.31b}$$

where $a_{21}$ is an additional constant.

Substituting Eq. (2.25b) into Eq. (2.25a) yields

$$Pv' + \frac{1}{2} h_b P' = 0. \tag{2.32}$$

Inserting Eq. (2.31a) into Eq. (2.32) leads to

$$v_1(x) = -\frac{1}{2} h_b [ln(a_{19} e^{\alpha_2 x} + {a_{20}}^{-\alpha_2 x})] + a_{22}, \tag{2.33}$$

where $a_{22}$ is an additional constant.

### *2.5.2 Solution in the second region:* $\mathbf{0 < x < r}$

Using Eq. (2.27b) in Eq. (2.25b) yields

$$P_2' = w G_a \frac{\eta}{h_a}, \tag{2.34}$$

which can be integrated to obtain

$$P_2(x) = w G_a \frac{\eta}{h_a} x + a_{23}, \tag{2.35a}$$

where $a_{23}$ is a constant.

Using Eq. (2.35a) in Eq. (2.29) and integrating the resulting equation will give

$$u_2(x) = \frac{G_a}{E_b h_b}\frac{\eta}{2h_a}x^2 + \frac{a_{23}}{E_b h_b}x + a_{24}, \tag{2.35b}$$

where $a_{24}$ is a constant.

Substituting Eq. (2.35a) into Eq. (2.32) leads to

$$v_2(x) = -\frac{1}{2}h_b\left[ln(wG_a\frac{\eta}{h_a}x + a_{23})\right] + a_{25}, \tag{2.35c}$$

where $a_{25}$ is an additional constant.

### *2.5.3 Solution in the third region: $r < x < q$*

The substitution of Eq. (2.27c) into Eq. (2.25b) leads to

$$P_3' = \frac{wG_a\eta\rho}{h_a(\rho-\Delta)} - \frac{wG_a\eta u_3}{h_a(\rho-\Delta)}. \tag{2.36}$$

Differentiating Eq. (2.36) and substituting Eq. (2.29) into the resulting equation will give

$$P_3'' + s^2\alpha^2 P_3 = 0, \tag{2.37a}$$

where

$$s^2 = \frac{\eta}{\rho-\Delta}, \quad \alpha^2 = \frac{G_a}{E_b h_b h_a}. \tag{2.37b}$$

The solution of Eq. (2.37a) is given by

$$P_3(x) = a_{26}\,cos(s\alpha x) + a_{27}\,sin(s\alpha x). \tag{2.38a}$$

where $a_{26}$ and $a_{27}$ are two constants.

Substituting Eq. (2.38a) into Eq. (2.29) and integrating the resulting equation will yield

$$u_3(x) = \frac{1}{E_b w h_b}\left[\frac{a_{26}}{s\alpha} sin(s\alpha x) - \frac{a_{27}}{s\alpha} cos(s\alpha x)\right] + a_{28}, \quad (2.38b)$$

where $a_{28}$ is another constants.

From Eqs. (2.32) and (2.38a), it follows that

$$v_3(x) = -\frac{1}{2} h_b [ln(a_{26}\, cos(s\alpha x) + a_{27}\, sin(s\alpha x))] + a_{29}, \quad (2.38c)$$

where $a_{29}$ is an additional constant.

## 2.6 Loading Mode III (mixed-mode)

In this case, both the normal and shear stresses are present. From Eqs. (2.1) - (2.3), it follows that

$$M'' + Sw - \frac{1}{2} h_b P'' = (Pv')'. \quad (2.39)$$

For small deformations with $v' \approx 0$, Eq. (2.39) reduces to

$$M'' + Sw - \frac{1}{2} h_b P'' = 0. \quad (2.40)$$

The following traction laws (see Fig. 2.5) are considered:

$$S(v) = \frac{k}{w} v_1, \;\; \tau_1(u) = G_a \frac{u_1}{h_a}, \;\; x < 0; \quad (2.41a)$$

$$S(v) = \frac{k f_1 (f_2 - v_2)}{w(f_2 - f_1)}, \;\; \tau_2(u) = \frac{G_a g_1 (g_2 - u_2)}{h_a (g_2 - g_1)}, \;\; \text{if } 0 < x < r. \quad (2.41b)$$

### *2.6.1 Solution in the first region: $x < 0$*

Substituting Eqs. (2.4a-c) and (2.41a) into Eqs. (2.2), (2.3) and (2.40) will give

$$E_b I_b {\phi_1}''' + k v_1 - \frac{1}{2} h_b {P_1}'' = 0, \quad (2.42)$$

$$P_1 - \frac{h_a h_b E_b}{G_a} P_1'' = 0, \quad (2.43)$$

$$k_s\mu A(-\frac{d\phi_1}{dx}+\frac{d^2v_1}{dx^2})=kv_1. \tag{2.44}$$

Eqs. (2.42)-(2.44) can be rewritten as

$$v_1{}^{(4)}+A_8v_1{}''+A_9v_1+A_{10}P_1=0, \tag{2.45}$$

$$A_{11}P_1''-P_1=0, \tag{2.46}$$

$$\phi_1'=v_1{}''+A_8v_1, \tag{2.47}$$

where

$$A_8\equiv-\frac{k}{k_s\mu A},\quad A_9\equiv\frac{k}{E_bI_b},\quad A_{10}\equiv-\frac{G_a}{2E_b{}^2I_bh_a},\quad A_{11}\equiv\frac{E_bh_bh_a}{G_a}. \tag{2.48a-d}$$

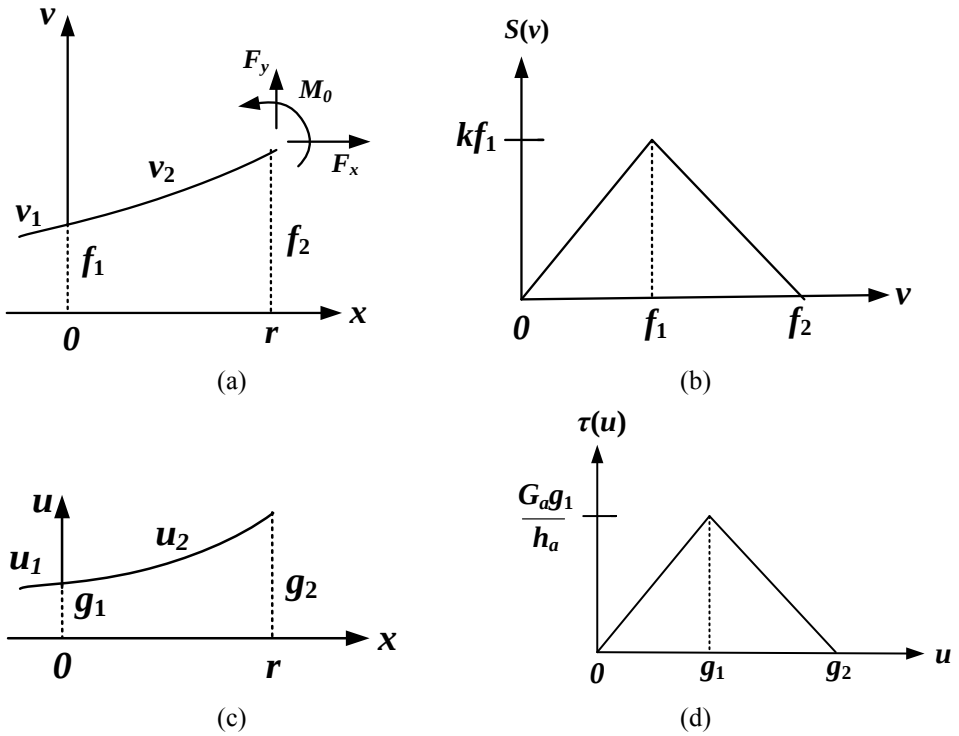


**Fig. 2.5** Loading in Mode III: (a) vertical displacement; (b) normal stress as a function of the vertical displacement; (c) horizontal displacement; (d) shear stress as a function of the horizontal displacement.

The general solutions of Eqs. (2.45)-(2.47) can be obtained as

$$P_1(x) = a_{30}e^{\lambda_1 x} + a_{31}e^{-\lambda_1 x}, \tag{2.49}$$

$$v_1(x) = a_{32}e^{\lambda_2 x} + a_{33}e^{-\lambda_2 x} + a_{34}e^{\lambda_3 x} + a_{35}e^{-\lambda_3 x} - \frac{A_{10}}{{\lambda_1}^4+A_8{\lambda_1}^2+A_9}\left(a_{30}e^{\lambda_1 x} + a_{31}e^{-\lambda_1 x}\right), \tag{2.50}$$

$$\begin{aligned}\phi_1(x) = {} & a_{32}\lambda_2 e^{\lambda_2 x} - a_{33}\lambda_2 e^{-\lambda_2 x} + a_{34}\lambda_3 e^{\lambda_3 x} - a_{35}\lambda_3 e^{-\lambda_3 x} - \frac{A_{10}}{{\lambda_1}^4+A_8{\lambda_1}^2+A_9}\left(a_{30}\lambda_1 e^{\lambda_1 x} - a_{31}\lambda_1 e^{-\lambda_1 x}\right) + A_8\left[\frac{a_{32}}{\lambda_2}e^{\lambda_2 x} - \frac{a_{33}}{\lambda_2}e^{-\lambda_2 x} + \frac{a_{34}}{\lambda_3}e^{\lambda_3 x} - \frac{a_{35}}{\lambda_3}e^{-\lambda_3 x} - \right. \\ & \left. \frac{A_{10}}{{\lambda_1}^4+A_8{\lambda_1}^2+A_9}\frac{1}{\lambda_1}\left(a_{30}e^{\lambda_1 x} - a_{31}e^{-\lambda_1 x}\right)\right] + a_{36}\,,\end{aligned} \tag{2.51}$$

where $a_{30}$~$a_{36}$ are constants, and

$$\lambda_1 \equiv \frac{1}{\sqrt{A_{11}}}\,,\ \lambda_2 \equiv \frac{1}{2}\sqrt{-2A_8 + 2\sqrt{{A_8}^2 - 4A_9}}\,,\quad \lambda_3 \equiv \frac{1}{2}\sqrt{-2A_8 - 2\sqrt{{A_8}^2 - 4A_9}}\,, \tag{2.52}$$

with ${A_8}^2 - 4A_9 \geq 0$ or $k \geq \frac{4{k_s}^2\mu^2A^2}{E_bI_b}$ assumed.

### *2.6.2 Solution in the second region:* $0 < x < r$

Substituting Eqs. (2.4a-c) and (2.41b) into Eqs. (2.2) (2.3) and (2.40) leads to

$$E_bI_b{\phi_2}''' + \frac{kf_1(f_2-v_2)}{(f_2-f_1)} - \frac{1}{2}h_b{P_2}'' = 0, \tag{2.53}$$

$$P_2 + \frac{h_ah_bE_b}{G_a}\frac{(g_2-g_1)}{g_1}P_2'' = 0, \tag{2.54}$$

$$k_s\mu A(-\frac{d\phi_2}{dx}+\frac{d^2v_2}{dx^2})=\frac{kf_1(f_2-v_2)}{(f_2-f_1)}. \tag{2.55}$$

Eqs. (2.53)-(2.55) can be rewritten as

$$v_2{}^{(4)}+A_{12}v_2{}''+A_{13}v_2+A_{14}P_2+A_{15}=0, \tag{2.56}$$

$$A_{16}P_2''+P_2=0, \tag{2.57}$$

$$\phi_2'=v_2{}''+A_{12}v_2+A_{17}, \tag{2.58}$$

where

$$A_{12}=\frac{kf_1}{k_s\mu A(f_2-f_1)},\quad A_{13}=-\frac{kf_1}{E_bI_b(f_2-f_1)},\quad A_{14}=\frac{G_a}{2E_b{}^2I_bh_a}\frac{g_1}{(g_2-g_1)},$$

$$A_{15}=\frac{kf_1f_2}{E_bI_b(f_2-f_1)},\qquad A_{16}=\frac{E_bh_bh_a}{G_a}\frac{(g_2-g_1)}{g_1},\quad A_{17}=-\frac{kf_1f_2}{k_s\mu A(f_2-f_1)}. \tag{2.59a-f}$$

The general solutions of Eqs. (2.56)-(2.58) give

$$P_2(x)=a_{37}cos(\lambda_4x)+a_{38}sin(\lambda_4x), \tag{2.60}$$

$$v_2(x)=$$

$$a_{39}e^{\lambda_5x}+a_{40}e^{-\lambda_5x}+a_{41}cos(\lambda_6x)+\ a_{42}sin(\lambda_6x)-\frac{A_{14}}{\lambda_4{}^4-A_{12}\lambda_4{}^2+A_{13}}[a_{37}cos(\lambda_4x)+$$

$$a_{38}sin(\lambda_4x)]-f_2, \tag{2.61}$$

$$\phi_2(x)=a_{39}\lambda_5e^{\lambda_5x}-a_{40}\lambda_5e^{-\lambda_5x}-a_{41}\lambda_6\,sin(\lambda_6x)+a_{42}\lambda_6\,cos(\lambda_6x)-$$

$$\frac{A_{14}}{\lambda_4{}^4-A_{12}\lambda_4{}^2+A_{13}}[-a_{37}\lambda_4sin(\lambda_4x)+a_{38}\lambda_4cos(\lambda_4x)]+A_{12}\left\{\frac{a_{39}}{\lambda_5}e^{\lambda_5x}-\frac{a_{40}}{\lambda_5}e^{-\lambda_5x}+\right.$$

$$\left.\frac{a_{41}}{\lambda_6}sin(\lambda_6x)-\frac{a_{42}}{\lambda_6}cos(\lambda_6x)-\frac{A_{14}}{\lambda_4{}^4-A_{12}\lambda_4{}^2+A_{13}}\left[\frac{a_{37}}{\lambda_4}sin(\lambda_4x)-\frac{a_{38}}{\lambda_4}cos(\lambda_4x)\right]-f_2x\right\}+$$

$$A_{17}x+a_{43}\ , \tag{2.62}$$

where $a_{37}$~$a_{43}$ are constants, and

$$\lambda_4 \equiv \frac{1}{\sqrt{A_{16}}}\,, \qquad \lambda_5 \equiv \frac{1}{2}\sqrt{-2A_{12} + 2\sqrt{{A_{12}}^2 - 4A_{13}}}\,,$$

$$\lambda_6 \equiv \tfrac{1}{2}\sqrt{-2A_{12} - 2\sqrt{{A_{12}}^2 - 4A_{13}}}\,. \tag{2.63a-c}$$

Furthermore, $\phi(x) = dv/dx$, then the kinematic relations given in Eqs. (2.4a-c) for a Timoshenko beam reduce to those for a Bernoulli-Euler beam [34]. With $\phi(x) = dv/dx$, the governing equation for the loading mode I given in Eq. (2.7) becomes

$$E_b I_b v'''' + wS = 0. \tag{2.64}$$

and then for the loading mode III give in Eq. (2.39)

$$E_b I_b v'''' + wS - \tfrac{1}{2} h_b P'' = (pv')'\,. \tag{2.65}$$

Eqs. (2.64) and (2.65) are those for the corresponding cases obtained in Plaut and Ritchie [23] based on the Bernoulli-Euler beam theory. This recovery verifies and supports the current formulation, which is more general.

**2.7 Numerical results and discussion**

To illustrate the analytical model developed in the preceding subsection, some sample cases have been studied quantitatively, with the numerical results shown graphically. The geometrical parameters are taken to be: $L$ = 10 mm, $h_a = 0.25$ mm, $h_b = 5$ mm, $w = 1$ mm. The adherend material is aluminium, and the adhesive is an epoxy. The properties of these two materials are $E_b = 75$ GPa, $G_a = 1$ GPa, $E_a =$ 2.5 GPa [15].

### *2.7.1 Loading Mode I*

In this case, the horizontal forces are not considered, and the solution is obtained in Eqs. (2.13a), (2.14), (2.18), (2.19), (2.23a) and (2.24). The boundary conditions needed to determine the 18 constants, $a_1 \sim a_{18}$ involved in the solution are identified as (see Figs. 2.1 and 2.3)

$$v_1 = 0,\ \ v_1' = 0,\ \ \phi_1 = 0,\ \ \phi_1{}' = 0\,,\ \ \phi_1{}'' = 0 \quad \text{at} \ \ x = -L,$$

$$v_1 = v_2 = c \quad \text{at} \quad x = 0,$$

$$v_2 = v_3 = z \quad \text{at} \quad x = r,$$

$$v_3 = d \quad \text{at} \quad x = q, \tag{2.66}$$

$$\text{Continuity of } \ \phi,\ \phi' \ \text{ and } \ v' \ \text{ at } x = 0 \text{ and } \ x = r,$$

$$\phi' = \frac{M_0}{E_b I_b} \ \text{ at } \ x = q,$$

$$(-\phi + v') = -\frac{F_y}{k_s \mu A} \ \text{ at } \ x = q.$$

For the case with $F_y = 20$ N, $M_0 = 10$ N $\cdot$ mm, $c = 1.17$ mm, $z = 1.46$ mm, $d = 2.05$ mm, $r = 0.141$ mm and $q = 0.390$ mm, the displacement and rotational angle are plotted in Figs. 2.6 and 2.7. From Fig. 2.6, it is seen that the vertical displacement is upward and increases monotonically with *x* in the cohesive zone in the current model which is predicted by the Timoshenko beam theory. It is also seen that the big difference between the current model and the Bernoulli-Euler beam theory based-model of Plaut and Ritchie [23] occurs approximately between $x = -4$ and $x = 0$ in the first region. The reason for the difference is the boundary conditions used. The current model considers the tape as a fixed end-free end beam which is suitable for short beams,

but the tape is assumed to be semi-infinite in the model of Plaut and Ritchie [23]. As shown in Fig. 2.7, the rotational angle has little minus value near the fixed-end edge and then increases smoothly and then starts to decrease near the peeling front. The normal stress predicted by the current model is plotted in Fig. 2.8, which is compared to that predicted by the model of Plaut and Ritchie [23]. The difference revealed in Fig. 2.8 is similar to that shown in Fig. 2.6.

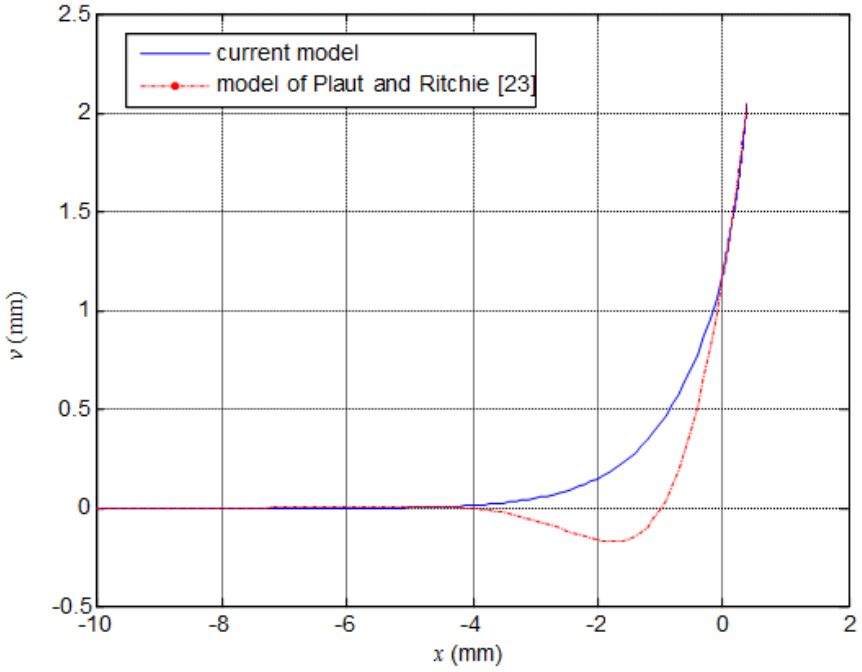


**Fig. 2.6** Vertical displacement $v$ under mode I loading.

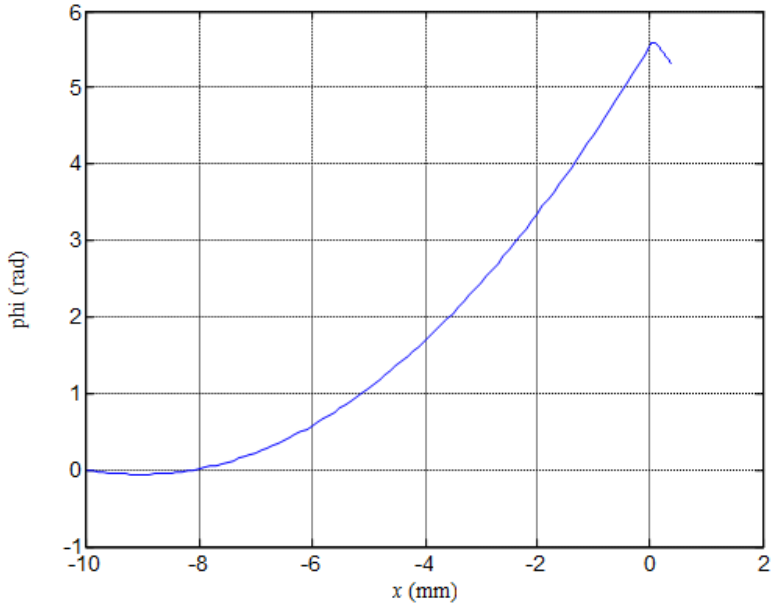


**Fig. 2.7** Rotational angle $\phi$ under mode I loading.

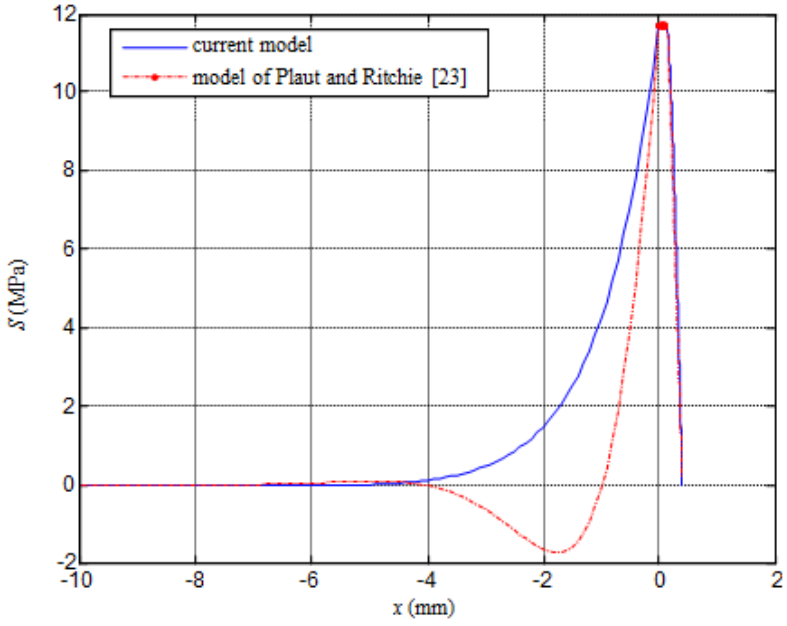


**Fig. 2.8** Normal stress under mode I loading.

To compare the experimental results of Christensen [57] with the predictions by the current model, the geometrical parameters are taken to be: $L$ = 2 mm, $h_a = 0.5$ mm, $h_b = 1$ mm, $w = 2$ mm. The adherend material is a steel (Tesa tape 4651), and the adhesive is a mixture of low- and high-molecular-weight polyisobutylenes. The elastic and shear moduli of these two materials on the adherend (with subscript b) and the adhesive (with subscript a) are, respectively, $E_b = 70$ GPa, $G_a = 0.43$ GPa, $E_a = 0.65$ GPa. The normal stresses in the adhesive predicted by the current model and those provided in Christensen [57] are displayed in Fig. 2.9. It is seen that the normal stress predicted by the current model exhibits a trend similar to that shown by the experimental data of Christensen [57] with both increasing monotonically with $x$. However, the slopes of the two curves are different. The reason for this discrepancy is that the peeling rate considered in the experimental study of Christensen [57] is non-zero, whereas the current model is peeling rate independent.

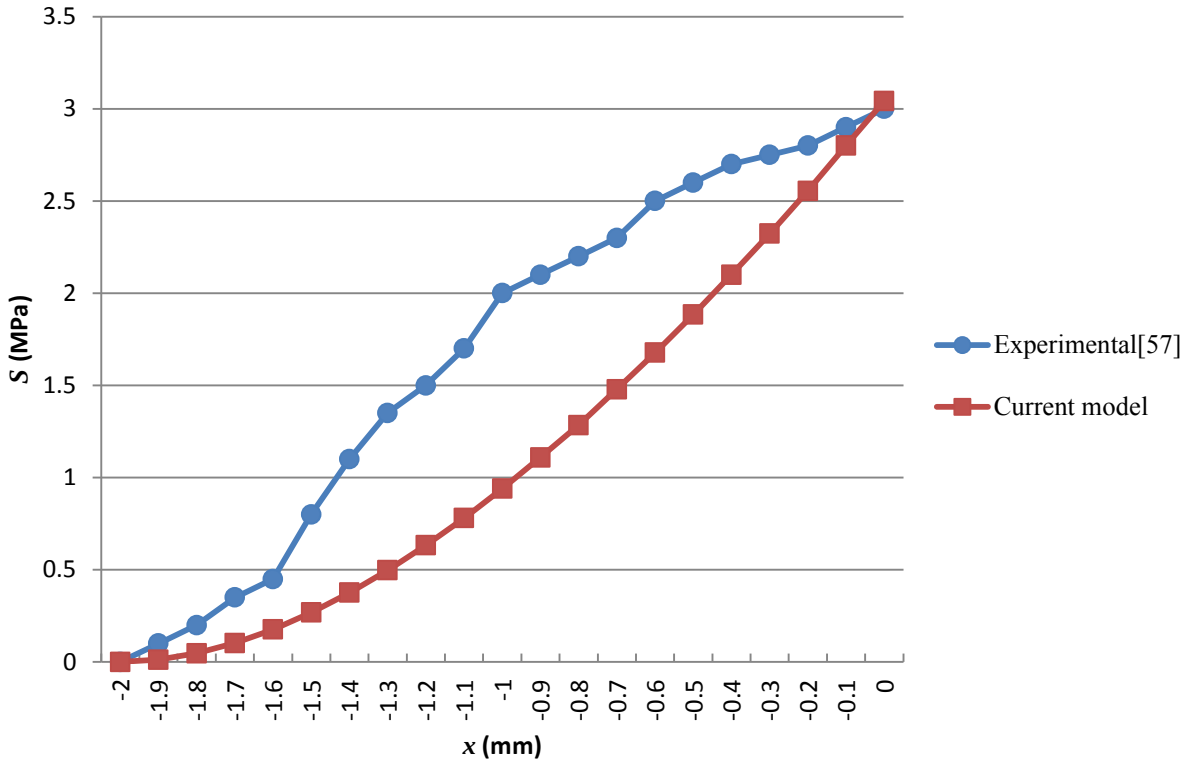


**Fig. 2.9** Comparison of the normal stresses under mode I loading.

### *2.7.2 Loading Mode II*

In this case, the solution are derived in Eqs. (2.31a,b), (2.33), (2.35a-c) and (2.38a-c). The 11 constants $a_{19}$~$a_{29}$ involved in the solution can be determined from the following boundary conditions (see Fig. 2.1 and 2.4):

$$u_1 = 0 \text{ at } x = -L,$$

$$u_1 = u_2 = \eta \text{ at } x = 0,$$

$$u_2 = u_3 = \Delta \text{ at } x = r,$$

$$u_3 = \rho \text{ at } x = q, \tag{2.67}$$

Continuity of $P$ and $P'$ at $x = 0$ and $x = r$,

$$P = \frac{F_x}{E_b w \, \mathrm{h}_b} \text{ at } x = q.$$

For $\Delta$ = 1.25 mm, $\rho$ = 1.75 mm, $r$ = 0.225 mm, $q$ = 0.595 mm, $F_x = \sqrt{200}$ N the horizontal displacement $u(x)$ is plotted in Fig. 2.10. The curve increases smoothly and is the same as that obtained in Plaut and Ritchie [23] using Bernoulli-Euler beam theory, as expected.

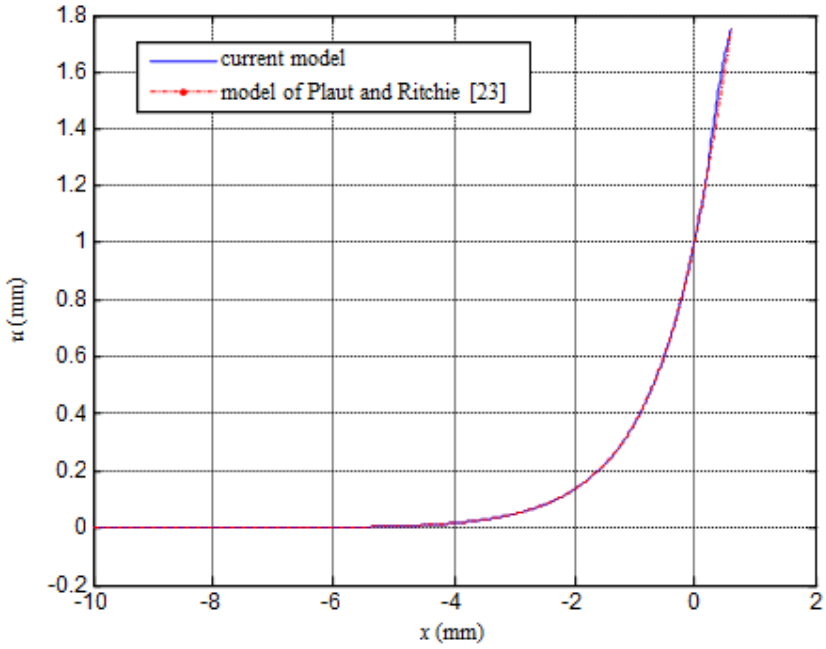


**Fig. 2.10** Horizontal displacement under mode II loading.

### *2.7.3 Lading Mode III*

In this case, the solution is given in Eqs. (2.49)-(2.51), and (2.60)-(2.62). The 14 constants $a_{30}$~$a_{43}$ involved in the solution are determined from the following boundary conditions (see Fig. 2.1 and 2.5):

$$v_1 = 0,\ \ v_1' = 0,\ \ \phi_1 = 0,\ \ \phi_1' = 0 \quad \text{at} \quad x = -L,$$

$$v_1 = v_2 = f_1 \quad \text{at } x = 0,$$

$$\text{Continuity of } v',\ \phi, \phi' \text{ at } x = 0,$$

$$\text{Continuity of } P \text{ and } P' \text{ at } x = 0, \tag{2.68}$$

$$P_2 = \frac{F_x}{E_b w\, \mathrm{h}_b},\ \ \phi' = \frac{M_0}{E_b I_b},\ \ \ (-\phi + v') = -\frac{F_y}{k_s \mu A} \ \text{ at } \ x = r.$$

For $r = 0.5$ mm, $F_x = 2$ N, $F_y = 4$ N and $M_0 = 2$ N $\cdot$ mm, the vertical displacement and rotational angle are illustrated in Figs. 2.11 and 2.12. It is observed from Fig. 2.11 that the vertical displacement increases significantly when $x > -1$ and then decreases near the peeling front. On the other hand, the rotational angle increases slowly with *x* and then decreases dramatically near the peeling front.

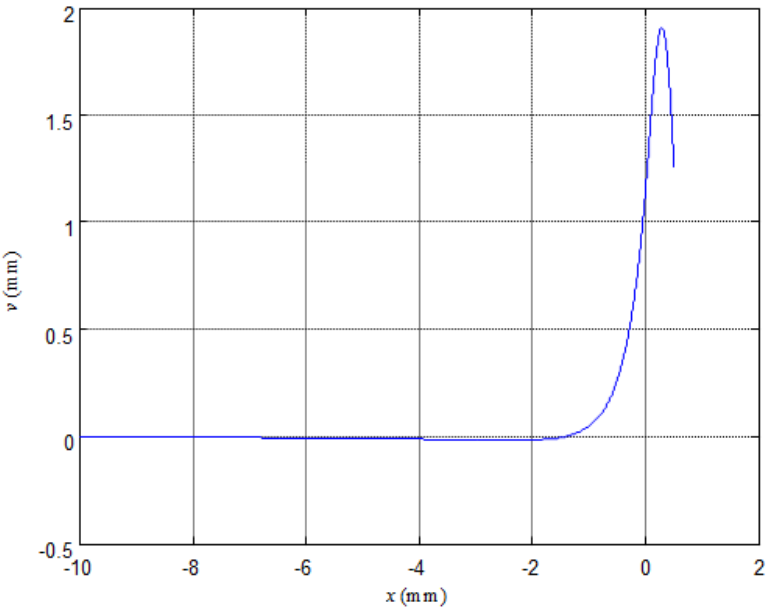


**Fig**. 2.11 Vertical displacement under mode III loading.

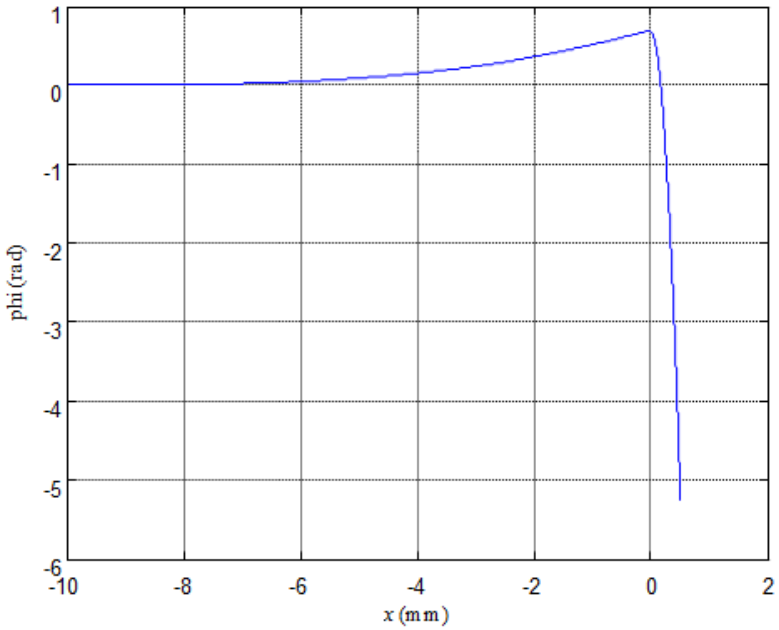


**Fig**. 2.12 Rotational angle under mode III loading.

# CHAPTER III

# PEELING TEST OF AN ADHESIVELY BONDED JOINT BASED ON A VISCOELASTIC BERNOULLI-EULER BEAM MODEL

## 3.1 Introduction

In this chapter, the adherend is modeled as a viscoelastic Bernoulli-Euler beam that is bonded to an elastic foundation. A configuration similar to that of Plaut and Ritchie [23] is considered. In Subsection 3.2, a brief introduction of viscoelastic behavior of materials is provided. A literature review of viscoelastic Bernoulli-Euler beam models is included in Subsection 3.3. The formulation is presented Subsection 3.4, where two cases are considered. The first is the case with a negligible shear stress in the adhesive (Mode I), while the second is the case with negligible normal stress in the adhesive (Mode II). The non-vanishing shear or normal stress in the adhesive in each case is assumed to have a step-stress history. The constitutive relations for the viscoelastic beam are derived by using the Boltzmann superposition integral in viscoelasticity and are then combined with the equilibrium equations to obtain governing equations. The Laplace transform method is used to solve the governing equations. Numerical results and discussion for the response of the viscoelastic beam under different temperatures are presented in Subsection 3.5.

### 3.2 Viscoelastic behavior of materials

Viscoelastic behavior of materials has been studied for a long time. The mathematical aspects of the subject have been well discussed in Christensen [35], Renady et al. [36] and Gurtin and Strengberg [37]. Linear viscoelasticity has been well elaborated in Bland [38] and Flugge [39], with an emphasis on mechanical models involving springs and dashpots. Golden and Graham [40] described various methods for solving boundary value problems in linear viscoelasticity.

Beam theories for viscoelastic materials can be developed by using the correspondence principle. The correspondence principle was proposed in 1950s (e.g., Alfrey [41], Read [42] and Lee [43]). Although a number of models have been published for viscoelastic beams having regular geometry and simple loading conditions, very few studies have been conducted to understand mechanical behavior of adhesive bonded joints using viscoelasticity due to the complexity, involved in the formulation. This motivated the work presented in the current chapter.

### 3.3 Bernoulli-Euler beam models for viscoelastic materials

Extending models for elastic beams to viscoelastic beams is challenging. Gurgoze [44] considered the dynamic stability of lateral vibrations of a simply supported viscoelastic beam and used Galerkin's method to obtain the governing partial differential equations. Olunloyo et al. [45] investigated the vibration damping in structures with layered viscoelastic beam-plates and formulated a boundary value problem using contact mechanics. Mofid et al. [46] provided two approaches, an analytical method based on

Laplace transforms and a discrete element method, for determining the dynamic behavior of viscoelastic beams with various boundary conditions. Nonlinear viscoelastic beams have also been studied. Argyris et al. [47] investigated chaotic vibrations of a nonlinear viscoelastic beam. Beldica and Hilton [48] analyzed the bending and piezoelectric control of a nonlinear viscoelastic beam.

### 3.4 Formulation

In this chapter, the configurations and free body diagrams are the same as those used in Chapter II, as shown in Figs. 2.1 and 2.2, but the origin of the coordinate system has been shifted to the left, as shown in Fig. 3.1. The difference is that the adherend is treated as a viscoelastic Bernoulli-Euler beam here. The shear or normal stress in the adhesive layer is assumed to have a step history.

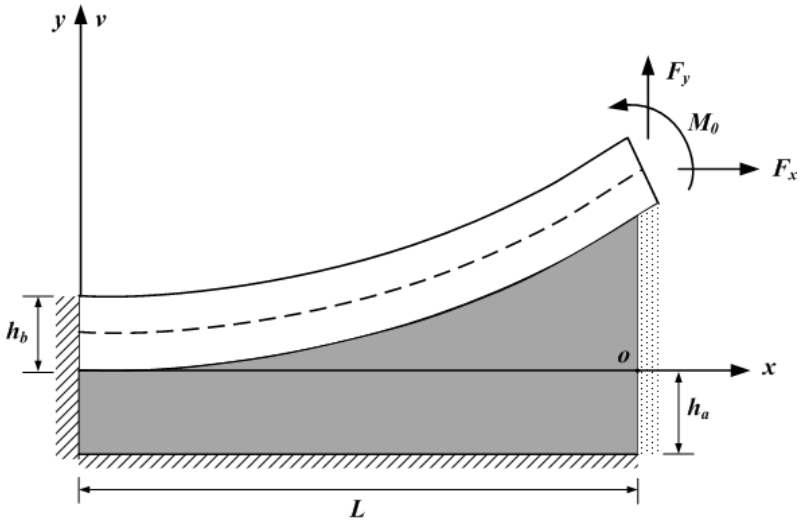


**Fig. 3.1** Schematic of a tape peeling test.

### *3.4.1 Loading Mode I*

In this mode, it is assumed that the horizontal forces are negligible such that $F_x$, $P$ and $\tau$ can all be set equal to zero. The equilibrium equations given in Eqs. (2.1)-(2.3) then become

$$\frac{\partial M}{\partial x} + Q = 0, \tag{3.1}$$

$$\frac{\partial Q}{\partial x} = Sw. \tag{3.2}$$

By using the Boltzmann superposition integral (e.g., Lakes [49]), the relation between the moment and deflection for a viscoelastic beam can be expressed as

$$M(x,t) = I_b \int_{0^-}^{t} \frac{\partial^2 v(x,t-\tau)}{\partial x^2} dE_b(\tau), \tag{3.3}$$

where $v$, $E_b$, $\mathrm{I_b}$ are, respectively, the vertical displacement, relaxation modulus and moment of inertia (with $I_b = h_b^3 w/12$) of the adherend.

Combining Eqs. (3.1) and (3.2) gives

$$\frac{\partial^2 M}{\partial x^2} + Sw = 0. \tag{3.4}$$

Consider a time-dependent normal stress *S* of the following form:

$$S = \frac{k}{w} H(t), \tag{3.5}$$

where *H(t)* is the Heaviside function. It then follows from Eqs. (3.4) and (3.5) that

$$I_b \int_{0^-}^{t} \frac{\partial^4 v(x,t-\tau)}{\partial x^4} dE_b(\tau) + kH(t) = 0. \tag{3.6}$$

Consider the beam deflection of the separation-of-variable form (e.g., [28, 51]):

$$v(x,t) = V(x)T(t). \tag{3.7}$$

Using Eq. (3.7) in Eq. (3.6) then gives

$$-\frac{I_b}{k}\frac{d^4V(x)}{dx^4} = \frac{H(t)}{\int_{0^-}^{t} T(t-\tau)dE_b(\tau)} = c_0, \tag{3.8}$$

where $c_0$ is a constant.

From Eq. (3.8), it follows that

$$\frac{d^4V(x)}{dx^4} = -\frac{k}{I_b}c_0. \tag{3.9}$$

The solution of Eq. (3.9) is

$$V(x) = -\frac{1}{24}\frac{k}{I_b}c_0x^4 + \frac{1}{6}\bar{c_1}x^3 + \frac{1}{2}\bar{c_2}x^2 + \bar{c_3}x + \bar{c_4}, \tag{3.10}$$

where $c_1 \sim c_4$ are constants.

Eq. (3.8) also says that

$$c_0\int_{0^-}^{t} T(t-\tau)dE_b(\tau) - H(t) = 0. \tag{3.11}$$

Taking the Laplace transform on Eq. (3.11) gives

$$c_0sE_b(s)T(s) - H(s) = 0. \tag{3.12}$$

It can be shown that (e.g., [49])

$$E_b(s)D(s) = \frac{1}{s^2}, \tag{3.13}$$

where $D(s)$ is the compliance in the transformed space.

Using Eq. (3.13) in Eq. (3.12) yields

$$c_0\frac{1}{sD(s)}T(s) - \frac{1}{s} = 0, \tag{3.14}$$

which gives

$$T(s) = \frac{1}{c_0}D(s). \tag{3.15}$$

Applying the Laplace transform then yields

$$T(t) = \frac{1}{c_0}D(t). \tag{3.16}$$

where $D(t)$ is the creep compliance in the time domain.

Substituting Eqs. (3.10) and (3.16) into Eq. (3.7) results in

$$v(x,t) = D(t)\left(\frac{-k}{I_b}\frac{1}{24}x^4 + \frac{1}{6}c_1x^3 + \frac{1}{2}c_2x^2 + c_3x + c_4\right). \tag{3.17}$$

where $c_1 \sim c_4$ are constants to be determined from boundary conditions.

For the peeling model with one end fixed and the other end free, the boundary conditions are

$$v(0,t) = 0, \quad \frac{\partial v(x,t)}{\partial x}\Big|_{x=0} = 0,$$

$$\frac{\partial v^3(x,t)}{\partial x^3}\Big|_{x=L} = \frac{-F_y}{E_b(t)I_b}, \quad \frac{\partial v^2(x,t)}{\partial x^2}\Big|_{x=L} = \frac{M_0}{E_b(t)I_b}. \tag{3.18a-d}$$

Using Eqs. (3.17) in Eqs. (3.18a-d) then yields

$$c_1 = \frac{1}{I_b}\left(-F_y + kL\right), \; c_2 = \frac{1}{I_b}\left(M_0 + F_yL - \frac{1}{2}kL^2\right), \; c_3 = 0, \; c_4 = 0. \tag{3.18e-h}$$

### *3.4.2 Loading Mode II*

In this case, $F_y$, $M_0$, $Q$, $M$ and $S$ are negligibly small such that they can all be set equal to be zero. Consider $\tau(x,t) = \frac{G_a}{h_a}\xi_0 H(t)$ caused by the applied horizontal force $F_x$. Similar to that in Chapter 2, the equilibrium equations now reduce to

$$P\frac{\partial v}{\partial x} + \frac{1}{2}wh_b\tau = 0, \tag{3.19a}$$

$$\frac{\partial P}{\partial x} = w\tau. \tag{3.19b}$$

By using the Boltzmann Superposition integral (e.g., [49]), the constitutive relation for the extensional deformation can be shown to be

$$P(x,t) = wh_b\int_{0^-}^{t}\frac{\partial u(x,t-\tau)}{\partial x}dE_b(\tau). \tag{3.20}$$

Consider the axial force $P(x,t)$ of the seperation-of-variable form:

$$P(x,t) = p_1(x)p_2(t). \tag{3.21}$$

Substituting Eq. (3.21) and $\tau(x,t) = \frac{G_a}{h_a}\xi_0 H(t)$ into Eq. (3.19b) gives

$$p_1{}'(x)p_2(t) = w\frac{G_a}{h_a}\xi_0 H(t). \tag{3.22}$$

From Eq. (3.22), $p_1(x)$ and $p_2(t)$ can be given as

$$p_1(x) = b_0 w\frac{G_a}{h_a}\xi_0 x + \bar{c_5}, \tag{3.23}$$

$$p_2(t) = \frac{1}{b_0}H(t), \tag{3.24}$$

where $b_0$ and $\bar{c_5}$ are two constants.

Then, it follows from Eqs. (3.21), (3.23) and (3.24) that

$$P(x,t) = \left(w\frac{G_a}{h_a}\xi_0 x + c_5\right)H(t). \tag{3.25}$$

where $c_5$ is a constant (with $c_5 \equiv \frac{\bar{c_5}}{b_0}$).

Similarly, consider the horizontal displacement of the form:

$$u(x,t) = U_1(x)U_2(t). \tag{3.26}$$

Using Eqs. (3.25) and (3.26) in Eq. (3.20) yields

$$\left(w\frac{G_a}{h_a}\xi_0 x + c_5\right)H(t) = wh_b\frac{\partial U_1(x)}{\partial x}\int_0^t U_2(t-\tau)dE_b(\tau). \tag{3.27}$$

From Eq. (3.27), it is seen that $U_1(x)$ is governed by

$$b_1\left(w\frac{G_a}{h_a}\xi_0 x + c_5\right) = wh_b\frac{\partial U_1(x)}{\partial x}, \tag{3.28}$$

which can be solved to obtain

$$U_1(x) = \frac{1}{wh_b}\left(\frac{1}{2}b_1 w\frac{G_a}{h_a}\xi_0 x^2 + \bar{c_6}x + \bar{c_7}\right), \tag{3.29}$$

where $b_1$, $\overline{c_6}$ and $\overline{c_7}$ are constants.

Also, it follows from Eq. (3.27) that

$$H(t) = b_1 \int_0^t U_2(t-\tau) dE_b(\tau), \tag{3.30}$$

Taking the Laplace transform on Eq. (3.30) gives

$$U_2(s) = \frac{1}{b_1} D(s), \tag{3.31}$$

which can be inverted to obtain

$$U_2(t) = \frac{1}{b_1} D(t). \tag{3.32}$$

From Eqs. (3.26), (3.29) and (3.32), it then follows that

$$u(x,t) = \left(\frac{1}{2}\frac{G_a}{h_a h_b}\xi_0 x^2 + c_6 x + c_7\right) D(t), \tag{3.33}$$

where $c_6$ and $c_7$ are two constants which can be determined from the following boundary conditions:

$$u(0,t) = 0, \qquad \frac{\partial u(x,t)}{\partial x}|_{x=l} = \frac{F_x}{E_b(t) w h_b}, \tag{3.34a,b}$$

as

$$c_6 = \frac{1}{h_b}\left(\frac{F_x}{w} - \frac{G_a \xi_0 L}{h_a}\right), \quad c_7 = 0. \tag{3.34c,d}$$

### 3.5 Numerical results and discussion

The three-parameter Kolrausch-Williams-Watts (KWW) model to compute the compliance $D(t)$ of the adherend (e.g., [50, 51]) will be used here. This model gives

$$D(t) = D^o e^{(\frac{t}{\tau})^\beta}. \tag{3.35}$$

where $D^o$, $\tau$ and $\beta$ are the initial compliance, retardation time and shape parameter, respectively. The values of these parameters are adopted from [50] and are listed in Table 3.1.

**Table3.1** Parameter values in the KWW model [50].

| T($^0$C) | D$^0$(1/GPa) | τ(sec.) | β |
|---|---|---|---|
| 200 | 0.133 | 1.56E+5 | 0.423 |
| 215 | 0.127 | 7.69E+4 | 0.315 |
| 230 | 0.118 | 2.83E+3 | 0.231 |

### *3.5.1 Loading Mode I*

The constants $c_1 \sim c_4$ involved in Eq. (3.17) are computed using Eqs. (3.18e-h). For the case with $F_y = 20$ N, $M_0 = 10$ N · mm, $E_a = 2.5$ GPa, $h_a = 0.25$ mm, $h_b = 5$ mm, $L = 10$ mm, $w = 1$ mm, the vertical displacement $v(x,t)$ at the free end $x = L$ is plotted in Fig. 3.2. Clearly, $v(L,t)$ monotonically increases with time and is larger at a higher temperature. Also, it is seen that at 230℃, $v(L,t)$ goes up rapidly, but at the other two lower temperatures it increases slowly.

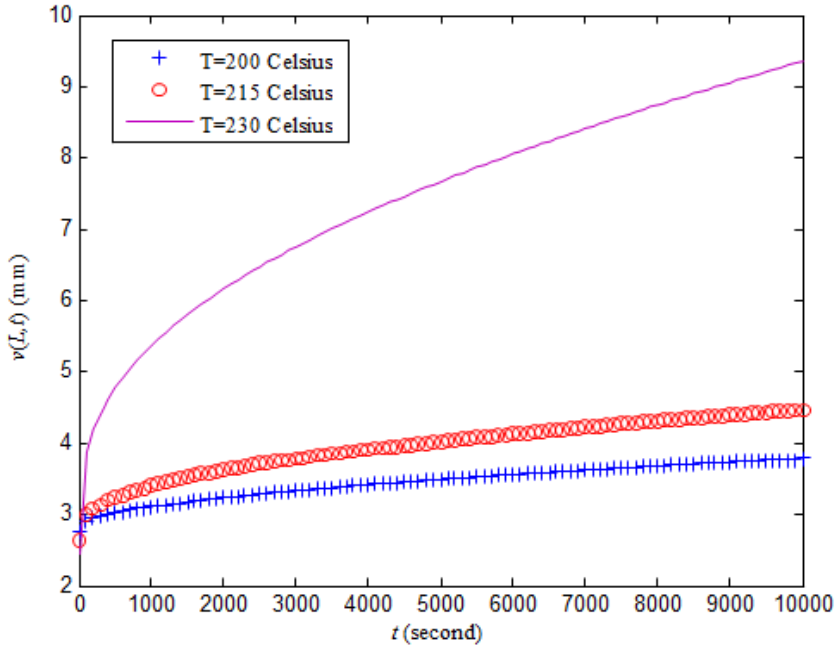


**Fig. 3.2** Vertical displacement at the free end $v(L,t)$ changing with time at different temperatures.

### *3.5.2 Loading Mode II*

In this case, Eqs. (3.33) and (3.34c,d) will be used to compute horizontal displacement, $u(x,t)$. The parameters values are taken to be $G_a = 1\ GPa$, $\xi_0 = 0.25$ mm, $F_x = 10$ N, $h_a = 0.25$ mm, $h_b = 5$ mm, $L = 10$ mm and $w = 1$ mm. The horizontal displacement at the free end, $u(L,t)$ is plotted in Fig. 3.3. It is seen that $u(L,t)$ increases monotonically with time $t$ and enlarges as temperature arises. This is similar to what is observed from Fig. 3.2 for $v(L,t)$ because both solutions are proportional to $D(t)$, as seen from Eqs. (3.17) and (3.33)

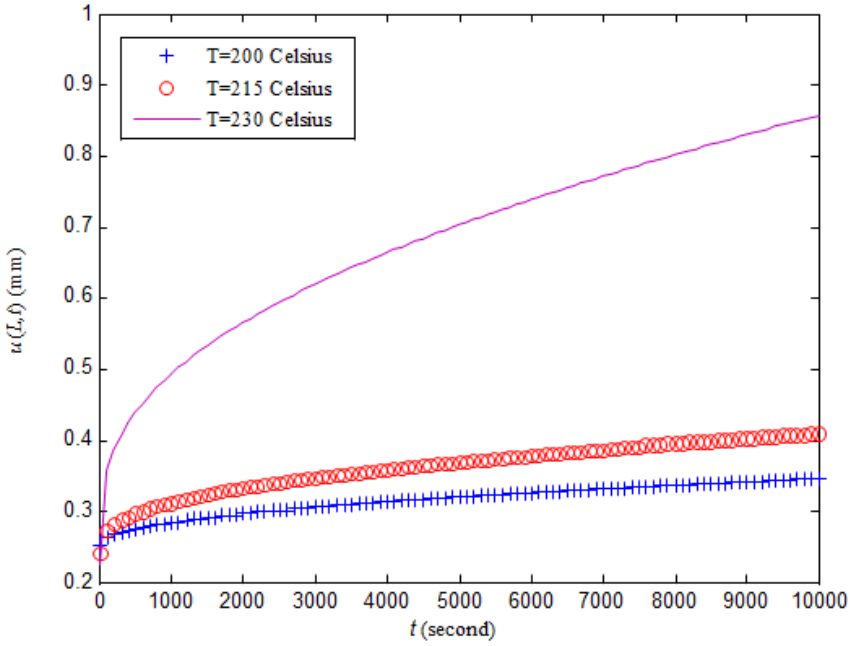


**Fig. 3.3** Horizontal displacement at the free end $u(L,t)$ changing with time at different temperatures.

# CHAPTER IV

# SYMMETRIC COMPOSITE ADHESIVELY BONDED JOINTS BASED ON THE TIMOSHENKO BEAM THEORY

## 4.1 Introduction

In this chapter, the Timoshenko beam theory is applied to model the adherend in the adhesive bonded joint, as was done in Chapter 2. However, the joint geometry and load distribution are different from those involved in the models developed in Chapter 2 and 3. The adherend is considered as a symmetric laminate. The adhesive layer is assumed to be homogeneous, isotropic and linearly elastic. To extend the existing models based on the classical laminate theory, the Timoshenko beam theory is employed in the formation here. The analytical solutions are obtained for both the adherends and adhesive layer. These solutions are applicable to various symmetric joint configurations. For given geometry and loading conditions of the joint, sample results are obtained by applying the newly derived solutions directly to quantitatively illustrate the stress distributions in the adherends and adhesive.

## 4.2 Symmetric composite adhesively bonded joints

Analytical solutions for adhesively bonded composite joints have been derived by employing the classical laminate theory [13, 15, 52]. There are many types of adhesive bonded joints, such as single-lap joint, single-strap joints, and stiffened joints. In Zou et al. [15], an analytical solution for a symmetric composite adhesively bonded

joint was provided by using the classical laminate theory and applied to various joint configurations. Also, a unified approach was presented by Mortensen and Thomsen [13] for different structural bonded joints involving elastic and viscoelastic adhesives. Analytical studies on nonlinear analysis of composite single-lap adhesive joints were conducted by Luo and Tong [11]. In addition, some authors [53, 54, 55, 56] have used the finite element method to analyze adhesive stresses in composite joints.

## 4.3 Analytical solution based on the Timoshenko beam theory

To extend the work of Zou et al. [15] based on the classical laminate theory and the Bernoulli-Euler beam model, the Timoshenko beam theory is employed in this study. The model is a symmetric composite joint subjected to in-plane and out-of plane loads as shown in Fig. 4.1. The solution is derived by following a procedure similar to that used in Zou et al. [15].

### *4.3.1 Kinematic and constitutive relations*

The displacement field based on the classical Timoshenko beam theory is given by [64]

$$u = u_o(x) - z\phi(x),\ v = 0\ ,\ w = w(x), \tag{4.1}$$

where $u_o(x)$, $w(x)$ are respectively, the *x*- and *z*- components of the displacement vector of the point $(x, 0, 0)$ on the centroidal axis of the beam, and $\phi$ is the angle of rotation (about the y-axis) of the cross-section with respect to the vertical direction.

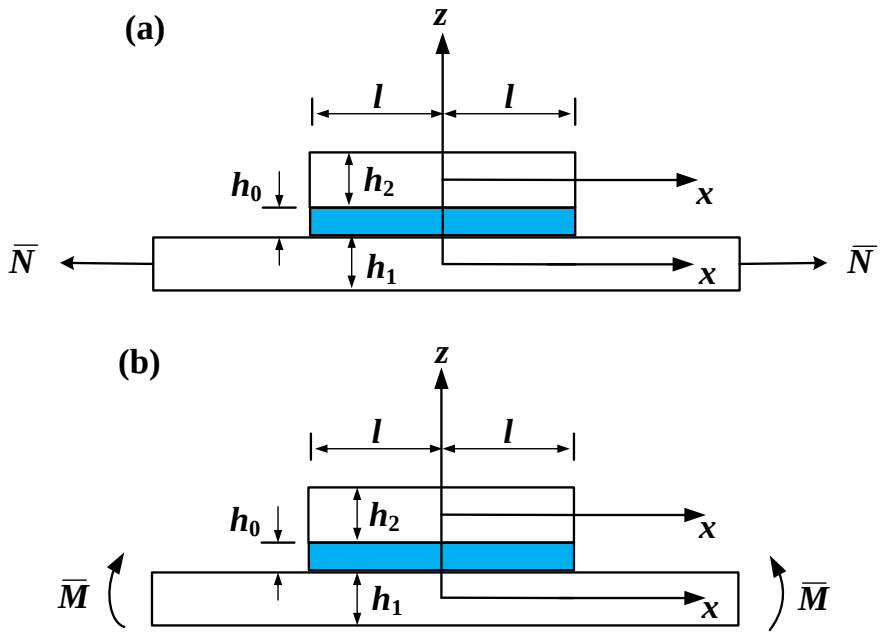


**Fig. 4.1** Symmetric composite joint under (a) axial tension forces and (b) bending moments.

The strain tensor is

$$\boldsymbol{\varepsilon} = \frac{1}{2}[\nabla \mathbf{u} + (\nabla \mathbf{u})^{\mathrm{T}}]. \tag{4.2}$$

From Eqs.(4.1) and (4.2), it follows that

$$\varepsilon_{xx} = u_{0,x} - z\phi_{,x},$$

$$\varepsilon_{xz} = \frac{1}{2}\left(-\phi + w_{,x}\right), \tag{4.3a-f}$$

$$\varepsilon_{yy} = \varepsilon_{zz} = \varepsilon_{xy} = \varepsilon_{yz} = 0.$$

The resultant normal force $N$, transverse shear force $Q$ , and bending moment $M$ are

$$N = \int_A \sigma_{xx} dA, \tag{4.4}$$

$$Q = \int_A \tau_{xz} dA, \tag{4.5}$$

$$M = \int_A \sigma_{xx} z dA, \tag{4.6}$$

where $A$ is the beam cross-sectional area.

According to Hooke's law, the stress-strain relations of each adherend can be expressed in terms of its stiffness coefficient $c_{ij}$ as

$$\{\sigma_i\} = [c_{ij}]\{\varepsilon_j\} \quad (i,j = 1,2,\dots,6). \tag{4.7a}$$

For the current beam model with $\varepsilon_{yy} = \varepsilon_{zz} = \varepsilon_{xy} = \varepsilon_{yz} = 0$ (see Eqs. (4.3c-f)) and $c_{16} = 0$, Eq.(4.7a) gives

$$\sigma_{xx} = c_{11}\varepsilon_{xx}\,, \tag{4.7b}$$

$$\tau_{xz} = 2c_{66}\varepsilon_{xz}\,. \tag{4.7c}$$

Substituting Eqs. (4.7b,c) and (4.3a,b) into Eqs. (4.4)-(4.6) results in

$$N = A_{11}u_{0,x} - B_{11}\phi_{,x}\,, \tag{4.8a}$$

$$Q = -C_{11}\phi + C_{11}w_{,x}\,, \tag{4.8b}$$

$$M = B_{11}u_{0,x} - D_{11}\phi_{,x}\,, \tag{4.8c}$$

where

$$A_{11} = b\int_{-h/2}^{h/2} c_{11}dz, \quad B_{11} = b\int_{-h/2}^{h/2} c_{11}z dz,$$

$$C_{11} = b\int_{-h/2}^{h/2} \mu dz, \qquad D_{11} = b\int_{-h/2}^{h/2} c_{11}z^2 dz, \tag{4.9}$$

where b and $h_i$ are, respectively, the adherend's width and thickness, $\mu$ is the shear modulus, and $c_{11}$ and $c_{66}$ are stiffness constants for an isotropic material in a plane stress state given by

$$c_{11} = \frac{E_b}{1-\nu^2}\,, \qquad c_{66} = \frac{1}{2}\mu = \frac{E_b}{(1+\nu)}. \tag{4.10}$$

### *4.3.2 Adhesive stresses*

Assume that the adhesive layer is homogeneous, isotropic and linearly elastic. Also, it is taken to be perfectly bonded to the two adherends.

The normal strain in the adhesive is

$$\varepsilon = \frac{w_2 - w_1}{h_0}, \tag{4.11}$$

and the shear strain in the adhesive is

$$\gamma = \frac{u_2 - u_1}{h_0} = \frac{u_{o2} + \frac{h_2}{2}\phi_2 - u_{o1} + \frac{h_1}{2}\phi_1}{h_0}, \tag{4.12}$$

where $w_1$, $w_2$ are, respectively, the vertical displacements at the bottom and top surfaces of the adhesive, and $u_1$, $u_2$ are, respectively, the horizontal displacements at the bottom and top surfaces of the adhesive. These are obtained from the corresponding values of the bottom and top adherends using the perfect bonding conditions.

Then, the constitutive equations in the adhesive can be obtained from Eqs. (4.11) and (4.12) and Hook's law as

$$\sigma_a = \frac{E_a}{h_0}(w_2 - w_1), \tag{4.13}$$

$$\tau_a = \frac{G_a}{h_0}\left(u_{o2} + \frac{h_2}{2}\phi_2 - u_{o1} + \frac{h_1}{2}\phi_1\right), \tag{4.14}$$

where $E_a$ and $G_a$ are, respectively, the Young's modulus and shear modulus of the adhesive layer, and $\sigma_a$, $\tau_a$ are the normal and shear stress components in the adhesive layer.

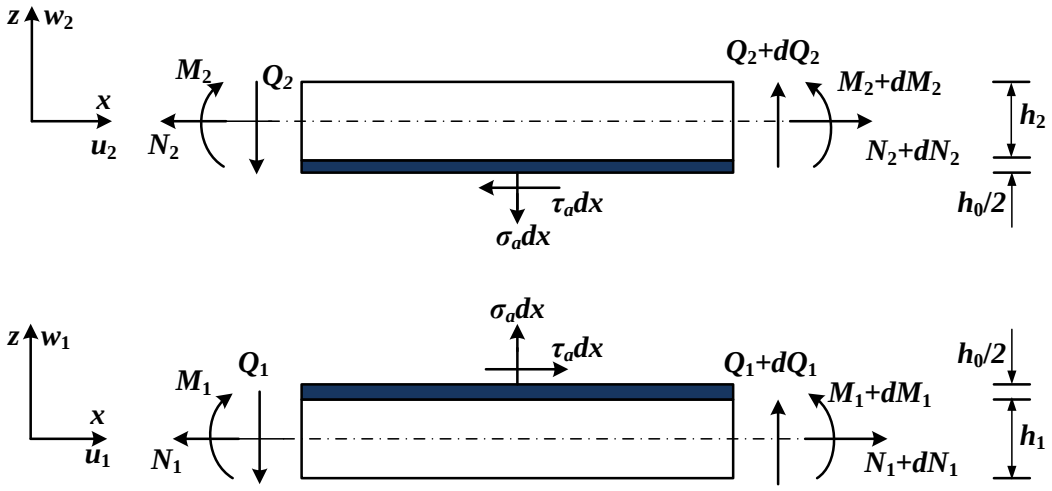


**Fig. 4.2** FBDs of differential elements of the adhesively bonded composite laminate.

### *4.3.3 Governing equations*

From the FBDs shown in Fig. 4.2, the equilibrium equations can be obtained from force and moment balance as

$$N_{1,x} = -b\tau_a,\ Q_{1,x} = -b\sigma_a,\ M_{1,x} = -Q_1 + b\frac{h_1+h_0}{2}\tau_a, \tag{4.15a-c}$$

$$N_{2,x} = b\tau_a,\ Q_{2,x} = b\sigma_a,\ M_{2,x} = -Q_2 + b\frac{h_2+h_0}{2}\tau_a, \tag{4.15d-e}$$

where $b$ is the width of the adherend.

From Eqs. (4.8a-c), it follows that

$$u_{o,x} = k_{11}N + k_{12}M\ , \tag{4.16}$$

$$\phi_{,x} = k_{13}N + k_{14}M\ , \tag{4.17}$$

$$w_{,x} = k_{15}Q + \phi. \tag{4.18a}$$

where

$$k_{11} = \frac{D_{11}}{A_{11}D_{11}-(B_{11})^2},\ k_{12} = \frac{-B_{11}}{A_{11}D_{11}-(B_{11})^2},$$

$$k_{13} = \frac{B_{11}}{A_{11}D_{11}-(B_{11})^2}, \quad k_{14} = \frac{-A_{11}}{A_{11}D_{11}-(B_{11})^2}, \quad k_{15} = \frac{1}{C_{11}}. \tag{4.18b}$$

Using Eqs. (4.15a-e), (4.16) and (4.17) in Eq. (4.14) leads to

$$\frac{d\tau_a}{dx} = \frac{G_a}{h_0}\left(\frac{du_{o2}}{dx} - \frac{du_{o1}}{dx} + \frac{h_2}{2}\frac{d\phi_2}{dx} + \frac{h_1}{2}\frac{d\phi_1}{dx}\right)$$

$$= \frac{G_a}{h_0}\left[\left(k_{11}^{(2)} + \frac{h_2}{2}k_{13}^{(2)}\right)N_2 + \left(k_{12}^{(2)} + \frac{h_2}{2}k_{14}^{(2)}\right)M_2 - \left(k_{11}^{(1)} - \frac{h_1}{2}k_{13}^{(1)}\right)N_1 - \left(k_{12}^{(1)} - \frac{h_1}{2}k_{14}^{(1)}\right)M_1\right], \tag{4.19}$$

$$\frac{d^2\tau_a}{dx^2} = \frac{G_a}{h_0}\left\{\left[k_{11}^{(2)} + k_{11}^{(1)} + \frac{h_2}{2}k_{13}^{(2)} - \frac{h_1}{2}k_{13}^{(1)} - \left(k_{12}^{(1)} - \frac{h_1}{2}k_{14}^{(1)}\right)\frac{h_1+h_0}{2} + \left(k_{12}^{(2)} + \frac{h_2}{2}k_{14}^{(2)}\right)\frac{h_2+h_0}{2}\right]\tau_a b - \left(k_{12}^{(2)} + \frac{h_2}{2}k_{14}^{(2)}\right)Q_2 + (k_{12}^{(1)} - \frac{h_1}{2}k_{14}^{(1)})Q_1\right\}, \tag{4.20}$$

$$\frac{d^3\tau_a}{dx^3} = \frac{G_a}{h_0}\left\{\left[k_{11}^{(2)} + k_{11}^{(1)} + \frac{h_2}{2}k_{13}^{(2)} - \frac{h_1}{2}k_{13}^{(1)} - \left(k_{12}^{(1)} - \frac{h_1}{2}k_{14}^{(1)}\right)\frac{h_1+h_0}{2} + \left(k_{12}^{(2)} + \frac{h_2}{2}k_{14}^{(2)}\right)\frac{h_2+h_0}{2}\right]b\frac{d\tau_a}{dx} - (k_{12}^{(2)} + \frac{h_2}{2}k_{14}^{(2)} + k_{12}^{(1)} - \frac{h_1}{2}k_{14}^{(1)})b\sigma_a\right\}, \tag{4.21}$$

$$\frac{d^3\tau_a}{dx^3} + \alpha_1\frac{d\tau_a}{dx} + \alpha_2\sigma_a = 0, \tag{4.22}$$

where

$$\alpha_1 \equiv -\frac{bG_a}{h_0}\left[k_{11}^{(2)} + k_{11}^{(1)} + \frac{h_2}{2}k_{13}^{(2)} - \frac{h_1}{2}k_{13}^{(1)} - \left(k_{12}^{(1)} - \frac{h_1}{2}k_{14}^{(1)}\right)\frac{h_1+h_0}{2} + \left(k_{12}^{(2)} + \frac{h_2}{2}k_{14}^{(2)}\right)\frac{h_2+h_0}{2}\right], \tag{4.23a}$$

$$\alpha_2 \equiv \frac{bG_a}{h_0}\left[k_{12}^{(2)} + \frac{h_2}{2}k_{14}^{(2)} + k_{12}^{(1)} - \frac{h_1}{2}k_{14}^{(1)}\right]. \tag{4.23b}$$

Similarly, it follows from Eqs. (4.15a-e), (4.17), (4.18a) and (4.13) that

$$\frac{d\sigma_a}{dx} = \frac{E_a}{h_0}\left(\frac{dw_2}{dx} - \frac{dw_1}{dx}\right)$$

$$= \frac{E_a}{h_0}\left[k_{15}^{(2)}Q_2 + \phi_2 - \left(k_{15}^{(1)}Q_1 + \phi_1\right)\right], \tag{4.24}$$

$$\frac{d^2\sigma_a}{dx^2} = \frac{E_a}{h_0}\left[\left(k_{15}^{(2)} + k_{15}^{(1}\right)b\sigma_a + \left(k_{13}^{(2)}N_2 - k_{13}^{(1)}N_1 + k_{14}^{(2)}M_2 - k_{14}^{(1)}M_1\right)\right], \tag{4.25}$$

$$\frac{d^3\sigma_a}{dx^3} = \frac{E_a}{h_0}\left[\left(k_{15}^{(2)} + k_{15}^{(1}\right)b\frac{d\sigma_a}{dx} + \left(k_{13}^{(2)} + k_{13}^{(1)} + \frac{h_2+h_0}{2}k_{14}^{(2)} - \frac{h_1+h_0}{2}k_{14}^{(1)}\right)b\tau_a + \left(-k_{14}^{(2)}Q_2 + k_{14}^{(1)}Q_1\right)\right], \tag{4.26}$$

$$\frac{d^4\sigma_a}{dx^4} = \frac{E_a}{h_0}\left[\left(k_{15}^{(2)} + k_{15}^{(1}\right)b\frac{d^2\sigma_a}{dx^2} + \left(k_{13}^{(2)} + k_{13}^{(1)} + \frac{h_2+h_0}{2}k_{14}^{(2)} - \frac{h_1+h_0}{2}k_{14}^{(1)}\right)b\frac{d\tau_a}{dx} - \left(k_{14}^{(2)} + k_{14}^{(1)}\right)b\sigma_a\right], \tag{4.27}$$

$$\frac{d^4\sigma_a}{dx^4} + \eta_1\frac{d^2\sigma_a}{dx^2} + \eta_2\frac{d\tau_a}{dx} + \eta_3\sigma_a = 0\,, \tag{4.28}$$

where

$$\eta_1 \equiv -\frac{bE_a}{h_0}\left(k_{15}^{(2)} + k_{15}^{(1}\right),\ \eta_2 \equiv -\frac{bE_a}{h_0}\left(k_{13}^{(2)} + k_{13}^{(1)} + \frac{h_2+h_0}{2}k_{14}^{(2)} - \frac{h_1+h_0}{2}k_{14}^{(1)}\right),$$

$$\eta_3 \equiv \frac{bE_a}{h_0}\left(k_{14}^{(2)} + k_{14}^{(1)}\right). \tag{4.29a-c}$$

When the adherends are made of symmetric and equal-thickness laminates $B_{11} = 0$ and thus $k_{12} = k_{13} = 0$. Also, when each adherend is made of the same material, $k_{14}^{(1)} = k_{14}^{(2)}$, and hence $\alpha_2 = 0$ and $\eta_2 = 0$. Therefore, the governing equations can be obtained from Eqs. (4.22) and (4.28), with $k_{12}^{(1)} = k_{12}^{(2)} = k_{13}^{(1)} = k_{13}^{(2)} = 0$, $\alpha_2 = 0$ and $\eta_2 = 0$

$$\begin{cases} \dfrac{d^3\tau_a}{dx^3} - \xi^2\dfrac{d\tau_a}{dx} = 0 \\ \dfrac{d^4\sigma_a}{dx^4} + \eta_1\dfrac{d^2\sigma_a}{dx^2} + \eta_3\sigma_a = 0 \end{cases} \tag{4.30a,b}$$

where

$$\xi^2 = -\alpha_1.$$

The general solution for Eqs. (4.30a,b) can be stated as

$$\tau_a = c_1 + c_2\, cosh(\xi x) + c_3\, sinh(\xi x), \tag{4.31}$$

$$\sigma_a = c_4 e^{\gamma_1 x} + c_5 e^{-\gamma_1 x} + c_6 e^{\gamma_2 x} + c_7 e^{-\gamma_2 x}, \tag{4.32}$$

where $c_1 \sim c_7$ are seven constants, and

$$\gamma_1 \equiv \frac{1}{2}\sqrt{-2\eta_1 + 2\sqrt{{\eta_1}^2 - 4\eta_3}}\ , \quad \gamma_2 \equiv \frac{1}{2}\sqrt{-2\eta_1 - 2\sqrt{{\eta_1}^2 - 4\eta_3}}\ . \tag{4.33a,b}$$

For the shear stresses in the adhesive, Eq. (4.31) is the same as that of Zou et al. [15]. However, the general solution for the normal stress in the adhesive given by Eq. (4.32) is different from that proposed by Zou et al. [15] due to the additional term $\eta_1 \frac{d^2\sigma_a}{dx^2}$ involved here in Eq. (4.30b), where $\eta_1$ contains the shear modulus, μ, as seen from Eqs. (4.29a), (4.18b) and (4.9).

### *4.3.4 Boundary conditions*

The boundary conditions are

$$\int_{-l}^{l} \tau_a(x)dx = N_1|_{x=-l} - N_1|_{x=l}\ , \tag{4.34a}$$

$$\int_{-l}^{l} \sigma_a(x)dx = Q_1|_{x=-l} - Q_1|_{x=l}\ , \tag{4.34b}$$

$$\int_{-l}^{l} \sigma_a(x)\cdot x dx = -M_1|_{x=l} + M_1|_{x=-l} - l\cdot Q_1|_{x=l} - l\cdot Q_1|_{x=-l} - \frac{h_1+h_0}{2}(N_1|_{x=l} - N_1|_{x=-l}), \tag{4.34c}$$

Also, it follows from Eqs. (5.19),(5.20), (5.25) and (5.26)

$$\frac{d\tau_a(x)}{dx}|_{x=l} = \frac{G_a}{h_0}\left[\left(k_{11}^{(2)} + \frac{h_2}{2}k_{13}^{(2)}\right)N_2|_{x=l} + \left(k_{12}^{(2)} + \frac{h_2}{2}k_{14}^{(2)}\right)M_2|_{x=l} - \left(k_{11}^{(1)} - \frac{h_1}{2}k_{13}^{(1)}\right)N_1|_{x=l} - \left(k_{12}^{(1)} - \frac{h_1}{2}k_{14}^{(1)}\right)M_1|_{x=l}\right], \tag{4.34d}$$

$$\frac{d^2\tau_a}{dx^2}|_{x=l} + \alpha_1\tau_a(x)|_{x=l} = \frac{G_a}{h_0}\left\{-\left(k_{12}^{(2)} + \frac{h_2}{2}k_{14}^{(2)}\right)Q_2|_{x=l} + (k_{12}^{(1)} - \frac{h_1}{2}k_{14}^{(1)})Q_1|_{x=l}\right\},$$

(4.34e)

$$\frac{d^2\sigma_a}{dx^2}|_{x=l} + \eta_1\sigma_a|_{x=l} = \frac{E_a}{h_0}\left[\left(k_{13}^{(2)}N_2|_{x=l} - k_{13}^{(1)}N_1|_{x=l} + k_{14}^{(2)}M_2|_{x=l} - k_{14}^{(1)}M_1|_{x=l}\right)\right],$$

(4.34f)

$$\frac{d^3\sigma_a}{dx^3}|_{x=l} + \eta_1\frac{d\sigma_a}{dx}|_{x=l} + \eta_2\tau_a|_{x=l} = \frac{E_a}{h_0}\left[\left(-k_{14}^{(2)}Q_2|_{x=l} + k_{14}^{(1)}Q_1|_{x=l}\right)\right].$$

(4.34g)

These seven boundary conditions will be used to determine the seven constants $c_1 \sim c_7$ involved in the solutions obtained in Eqs. (4.31) and (4.32). This is done numerically next.

**4.4 Numerical results and discussion**

In this subsection, two cases are investigated with each adherend being a cross-ply symmetric laminate (i.e.,$[0^\circ, 0^\circ, 90^\circ]_s$) of a glass fiber reinforced polymer (GFRP) matrix composite. The two identical laminates are jointed (bonded) by an expoxy adhesive. The material properties of the adherend and the adhesive are summarized in Table 4.1.

The thickness of the adherends, $h_b$, and the thickness of adhesive layer, $h_a$ are fixed at 5 mm and 0.25 mm, respectively. The bonded composite joint has an overlap length of 2*l* = 50 mm and a width *b* = 1 mm. (see Fig. 4.1)

**Table 4.1** Mechanical properties of the materials used [15].

| Property/material | GFRP | Adhesive |
|---|---|---|
| Young's modulus (GPa) | $E_1 = 30$ | 2.5 |
| | $E_2 = 6.0$ | |
| Poisson's ratio | $\nu_{12} = 0.30$ | 0.25 |
| | $\nu_{21} = 0.06$ | |
| Shear modulus (GPa) | 4.5 | 1.0 |

### *4.4.1 Adhesively bonded composite laminate under uniaxial tension*

In this case (see Fig. 4.1(a)), the adhesively bonded composite laminate is subjected to the tensile load $\bar{N}$ = 100 N only. Then the constants $c_1 \sim c_7$ involved in Eqs. (4.31) and (4.32) are determined from Eqs. (4.34a)-(4.34g) with the following conditions:

$$N_2|_{x=l} = M_2|_{x=l} = Q_2|_{x=l} = M_1|_{x=-l} = M_1|_{x=l} = Q_1|_{x=-l} = Q_1|_{x=l} = 0,$$

$$N_1|_{x=l} = \bar{N}, \quad N_2|_{x=-l} = \bar{N}. \tag{4.35a}$$

Then, the shear stress can be obtained as

$$\tau(x) = \frac{-G_a k_{11} \bar{N}}{\xi h_0 cosh(\xi l)} sin\, h(\xi x). \tag{4.35b}$$

which is identical to the expression using Bernoulli-Euler beam theory-based model of Zou et al. [15].

The normal stress in the adhesive vanishes in this case due to the specific loading. The shear stress in the adhesive predicted by the current model is shown in Fig.

4.3, where it is also compared to that predicted by the Bernoulli-Euler beam theory-based model of Zou et al. [15]. It is seen that two models match extremely well, as expected. This is because the solution for the shear stress in the adhesive is the same, as mentioned earlier.

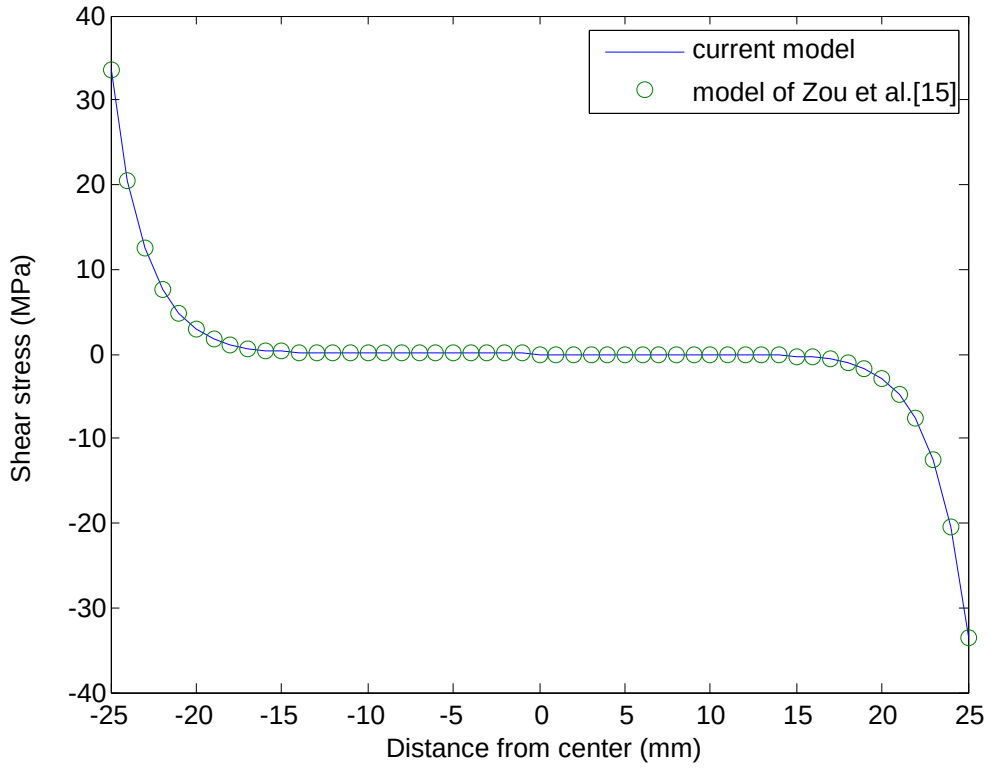


**Fig. 4.3** Shear stress in the adhesive of the composite joint subjected to uniaxial tension.

### *4.4.2 Adhesively bonded composite laminate under pure bending moment*

In this case, only a pair of bending moments $\bar{M} = 100\ N \cdot mm$ is applied (see Fig. 4.1(b)). The constants $c_1 \sim c_7$ involved in Eqs. (4.31) and (4.32) are determined from Eqs. (4.34a-g) with the following conditions:

$$N_2|_{x=l} = N_1|_{x=l} = Q_2|_{x=l} = N_1|_{x=-l} = N_1|_{x=l} = Q_1|_{x=-l} = Q_1|_{x=l} = 0,$$

$$M_1|_{x=l} = \bar{M}, \quad M_1|_{x=-l} = \bar{M}. \tag{4.36a}$$

Therefore, the shear stress can be expressed as

$$\tau(x) = \frac{-G_a k_{14} h \bar{M}}{2\xi h_0 cosh(\xi l)} sin\, h(\xi x), \tag{4.36b}$$

where $h = h_1 = h_2$, $k_{14} = k_{14}^{(1)} = k_{14}^{(2)}$.

Also, the shear stress derived in this case is the same as that is obtained by Zou et al. [15].

The shear and normal stresses in the adhesive predicted by the current Timoshenko beam theory-based model, respectively, displayed in Fig. 4.4 and Fig. 4.5, where they are also compared to those predicted by the Bernoulli-Euler beam theory-based model of Zou et al. [15]. From Fig. 4.4, it is seen that the shear stress results predicted by the two models are in a good agreement, as expected. However, a large difference exists between the two sets of predicted values for the normal stress near its two ends in the adhesive as shown in Fig. 4.5, which results from the transverse shear effect, as can be seen from Eq. (4.30b).

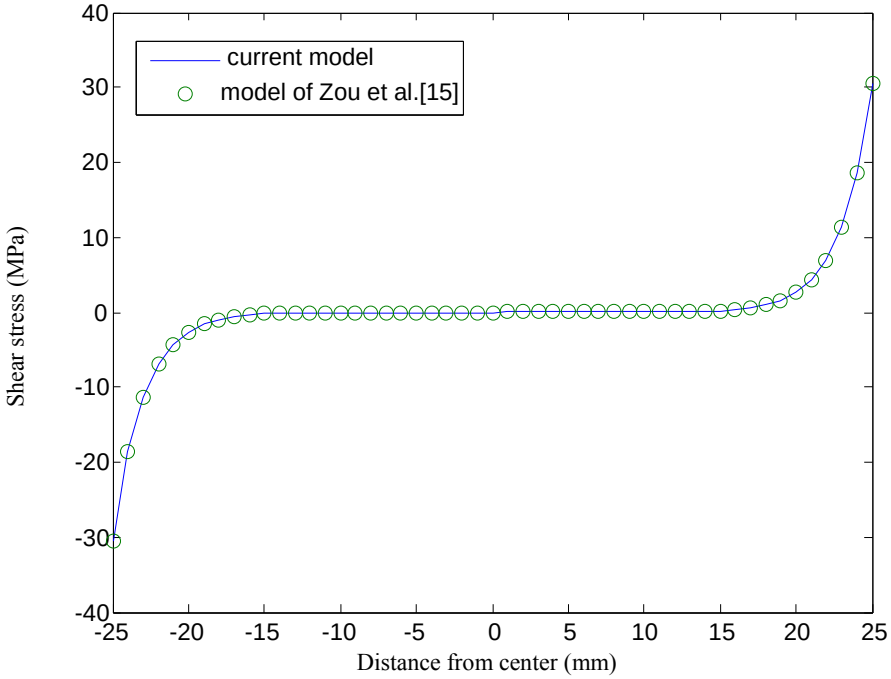


**Fig. 4.4** Shear stress in the adhesive of the composite joint subjected to pure bending.

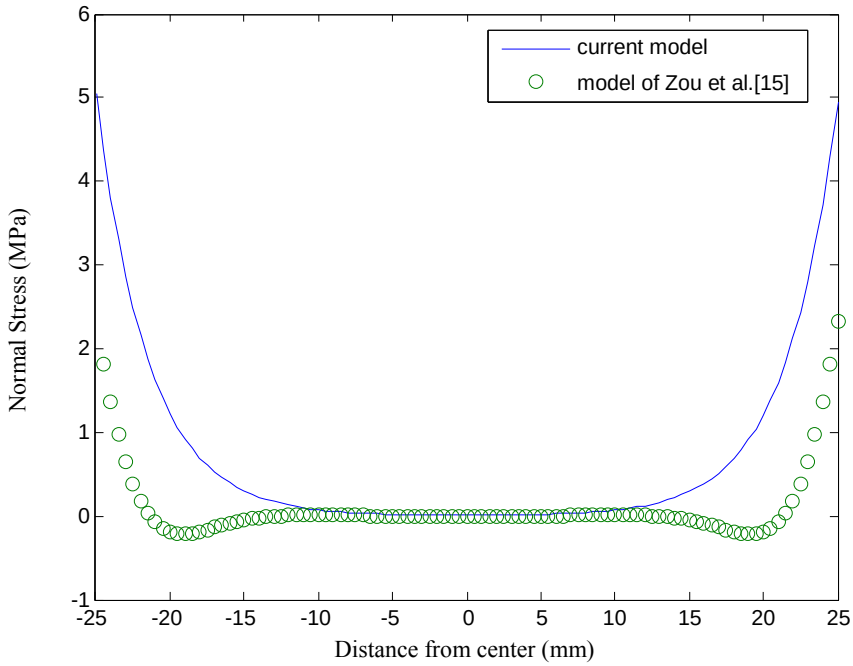


**Fig. 4.5** Normal stress in the adhesive of the composite joint subjected to pure bending.

# CHAPTER V

# SUMMARY

Two analytical solutions for the peeling test of adhesively bonded joints are derived in this thesis work using the classical Timoshenko beam theory for elastic materials and a Bernoulli-Euler beam model for viscoelastic materials, respectively. In addition, an analytical solution for a symmetric composite adhesively bonded joint is obtained by employing the Timoshenko beam theory.

In Chapter II, the peeling test of an adhesively bonded joint is represented using the model of a Timoshenko beam on an elastic foundation. Three cases are considered: (1) only the normal stress is acting (mode I); (2) only the transverse shear stress is present (mode II); and (3) the normal and shear stresses co-exist (mode III) in the adhesive. In mode I and mode III, the numerical results show that the vertical displacement increases smoothly for $x < 0$ and displays kinks near the peeling front. Furthermore, a comparison of the normal stress and vertical displacement under mode I loading shows a difference between the current model and a Bernoulli-Euler beam theory based-model in the first region due to different boundary conditions. Another comparison of the current model with the experimental results of Christensen is also made, which shows similar trends for the normal stress. The horizontal displacement under mode II loading is seen to be the same as that based on the Bernoulli-Euler beam theory, as expected.

In Chapter III, the peeling test is studied by regarding the adherend as a viscoelastic Bernoulli-Euler beam. The constitutive relations for viscoelastic beam are derived by using the Boltzmann superposition integral in viscoelasticity and are combined with equilibrium equations to obtain the governing equations. In the numerical analysis, the Kolraush-Williams-Watts (KWW) model is used to compute the compliance. The numerical results show that the vertical displacement increases as time and temperature increase, as expected.

In Chapter IV, the Timoshenko beam theory is employed to analytically study a symmetric composite adhesively bonded joint. The analytical solution derived here gives the shear stress in the adhesive which is the same as that obtained using the classical laminate theory. However, the normal stress in the adhesive is different due to the consideration of the transverse shear effect in the current model. This is also quantitatively illustrated in the numerical results.

# REFERENCES

[1] Volkersen O. Die Nietkraftverteilung in Zugbeanspruchten Nietverbindungen mit Konstanten Laschenquerschnitten. Luftfahrtforschung 1938;15:41-7.

[2] Goland M, Reissner E. The stress in cemented joints. J Appl Mech 1944;11:17-27.

[3] Hart-Smith LJ. Adhesive-bonded single-lap joints. NASA 1973;CR-112236.

[4] Oplinger, DW. A layered beam theory for single-lap joints. US Army Materials Technology Laboratory Report MTL TR 1991.

[5] Adams RD, Wake WC. Structural adhesive joints in engineering. Essex, England: Elsevier Applied Science Publishers Ltd; 1984.

[6] Tsai MY, Morton J. A note on peel stresses in single-lap adhesive joints. J Appl Mech 1994;712–715.

[7] Adams RD, Peppiatt NA. Effect of Poisson's ratio strains in adherents on stresses of idealized lap joint. J Strain Anal 1973;8:134–139.

[8] Adams RD, Peppiatt NA. Stress analysis of adhesive-bonded lap joints. J Strain Anal 1974;9:185–196.

[9] Allman DJ. A theory for the elastic stresses in adhesive bonded lap joints. Quarterly Journal of Mechanics and Applied Mathematics 1977;30:415-436.

[10] Chen D, Cheng S, Shi YP. An analysis of adhesive-bonded joints with nonidentical adherents. J Eng Mech 1991;117:605-623.

[11] Luo Q, Tong L. Analytical solutions for nonlinear analysis of composite single-lap adhesive joints. International Journal of Adhesion and Adhesives 2009;29:144-154.

[12] Thomsen OT. Elasto-static and elasto-plastic stress analysis of adhesively bonded tubular lap joints. Composite Structures 1992;21:249-259.

[13] Mortensen F, Thomsen OT. Analysis of adhesive bonded joint: a unified approach. Composites Science and Technology 2002;62:1011-1031.

[14] Luo Q, Tong L. Linear and higher order displacement theories for adhesively bonded lap joints. International Journal of Solids and Structures 2004;41:6351-6381.

[15] Zou GP, Shahin K, Taheri F. An analytical solution for the analysis of symmetric composite adhesively bonded joints. Composite Structures 2004;65:499-510.

[16] Crocombe AD, Adams RD. Peel analysis using the F-E method. Journal of Adhesion 1981;12:127-139.

[17] Kaelble DH. Theory and analysis of peel adhesion: Mechanisms and Mechanics. Transactions of the Society of Rheology 1959;3:161-182.

[18] Kaelble DH. Theory and analysis of peel adhesion: bond stresses and distribution. Transactions of the Society of Rheology 1960;4:45-73.

[19] Crocombe AD, Adams RD. An elasto-plastic investigation of the peel test. Journal of Adhesion 1982;13:241-267.

[20] Yamada SE. Elastic/plastic fracture analysis for bonded joints. Eng Fracture Mechanics 1987;27:315-328.

[21] Williams JG, Hadavinia H. Analytical solutions for cohesive zone models. J Mech. Phys Solids 2002;50:809-825.

[22] Georgiou I, Hadavinia H, Ivankovic A, Kinloch AJ, Tropsa V, Williams JG. Cohesive zone models and the plastically deforming peel test. J. Adhesion 2003;79: 239-265.

[23] Plaut RH, Ritchie JL. Analytical solutions for peeling using beam-on-foundation model and cohesive zone. The Journal of Adhesion 2004;80:313-331.

[24] Her SC. Stress analysis of adhesively-bonded lap joints. Composites Structures 1999;47:673-678.

[25] Chang FSC. The peeling force of adhesive joints. Transactions of the Society of Rheology 1960;4:75-89.

[26] Yang QD, Thouless MD, Ward SM. Elastic-plastic mode-II fracture of adhesive joints. Int J Solids Structure 2001;38:3251-3262.

[27] Yang QD, Thouless MD, Ward SM. Numerical simulations of adhesively-bonded beams failing with extensive plastic deformation. Journal of the Mechanics and Physics of Solids 1999;47:1337-1353.

[28] Yang QD, Thouless MD, Ward SM. Analysis of the symmetrical 90º-peel test with extensive plastic deformation. J Adhesion 2000;72:115-132.

[29] Thouless MD, Yang QD. In: The Mechanics of Adhesion, D. A. Dillard and A. V. Pocius. Eds. Elsevier: Amsterdam; 2002:235-217.

[30] Wei Y, Hutchinson, JW. Interface strength, work of adhesion and plasticity in the peel test. Int. J. Fracture 1998;93:315-333.

[31] Blackman BRK, Kinloch AJ, Paraschi M, Teo WS. Measuring the mode I adhesive fracture energy, $G_{IC}$,of structural adhesive joints: the results of an international round-robin. International Journal of Adhesion & Adhesives 2003;23:293–305.

[32] Blackman BRK, Kinloch AJ, Paraschi M. The determination of the mode II adhesive fracture resistance, $G_{IIC}$, of structural adhesive joints: an effective crack length approach. Engineering Fracture Mechanics 2005;72:877–897.

[33] Marannano GV, Mistretta L, Cirello A, Past S. Crack growth analysis at adhesive–adherent interface in bonded joints under mixed mode I/II. Engineering Fracture Mechanics 2008;75:5122–5133.

[34] Ma HM, Gao X.-L, Reddy JN. A microstructure-dependent Timoshenko beam model based on a modified couple stress theory. Journal of the Mechanics and Physics of solids 2008:3379-3391.

[35] Christensen RM. Theory of viscoelasticity. New York: Academic Press; 1982.

[36] Renady M, Hrus W, Nohel WJ. Mathematical problems in viscolasticity. New York: John Wiley; 1987.

[37] Gurtin ME, Strengberg E. On the linear theory of viscoelasticity. Arch Ration Mech Anal 1962;11:291–356.

[38] Bland DR. The theory of linear viscoelasticity. Oxford: Pergamon; 1960.

[39] Flugge W. Viscoelasticity. Waltham (MA): Blaisdell; 1967.

[40] Golden JM, Graham GA. Boundary value problems in linear viscoelasticity. Berlin: Springer Verlag; 1988.

[41] Alfrey T. Non-homogeneous stresses in viscoelastic media. Q. Appl. Math

II 1944:113-119.

[42] Read WT. Stress analysis for compressible viscoelastic materials. J Appl Phys 1950;21:671-674.

[43] Lee EH. Stress analysis in viscoelastic bodies. Q. Appl. Math. 1955;13:183-190.

[44] Gurgoze M. Parametric vibrations of a viscoelastic beam (Maxwell model) under steady axial load and transverse displacement excitation at one end. Journal of Sound and Vibration 1987;115:329-338.

[45] Olunloyo VOS, Osheku CA, Damisa O. Vibration damping in structures with layered viscoelastic beam-plate. Journal of Vibration and Acoustics 2008;130(061002): 1-26.

[46] Mofid M, Tehranchi A, Ostadhossein A. On the viscoelastic beam subjected to moving mass. Advances in Engineering Software 2010;41:240-247.

[47] Argyris J, Belubekian V, Ovakimyan N, Minasyan M. Chaotic vibrations of a nonlinear viscoelastic beam. Chaos, Solitons & Fractals 1996;7(2):151-163.

[48] Beldica CE, Hilton HH. Nonlinear viscoelastic beam bending with piezoelectric control – analytical and computational simulations. Composite Structures 2001;51: 195-203.

[49] Lakes RS. Viscoelastic Solids. CRC Press; 1998.

[50] Gates TS, Veazie DR, Brinson LC. Creep and Physical Aging in a Polymeric Composite: Comparison of Tension and Compression. Journal of Composite Materials 1997;31:2478-2505.

[51] Li K, Gao, X.-L, Roy AK. Micromechanical modeling of viscoelastic properties of carbon nanotube-reinforced polymer composites. Mechanics of Advanced Materials and Structures 2006;13:317-328.

[52] Crocombe AD, Ashcroft IA. Modeling of adhesively bonded joints. Berlin Heidelberg: Springer-Verlag; 2008.

[53] Adams RD, Peppiatt NA. Stress analysis of adhesive-bonded lap joints. Journal of Strain Analysis 1974;9:185-196.

[54] Sharifi S, Choupani N. Stress analysis of adhesively bonded double-lap joints subjected to combined loading. World Academy of Science, Engineering and Technology 2008;41:759-763.

[55] Rao MV, Rao KM, Raju VRC, Murthy VBK, Raju VVS. Analysis of adhesively bonded single-lap joint in laminated FRP composites subjected to transverse load. International Journal of Mechanics and Solids 2008;3:75-86.

[56] Richardson G, Crocombe AD, Smith PA. A comparison of two- and three-dimensional finite element analyses of adhesive joints. Int. J. Adhesion and Adhesives 1993;13:193-200.

[57] Christensen SF, Everland H, Hassager O, Almdal K. Observations of peeling of a polyisobutylene-based pressure-sensitive adhesive. International Journal of Adhesion and Adhesives 1998;18:131-137.

# VITA

Name: Ying-Yu Su

Address: Texas A&M University

Department of Mechanical Engineering

3123 TAMU

College Station TX 77843-3123

Email Address: candy010106@gmail.com

Education: B.S., Mechanical Engineering, National Chung Hsing University, Taichung, Taiwan, 2008

M.S., Mechanical Engineering, Texas A&M University, 2010